2-P

Tyco Laboratories, Inc.
Bear Hill
Waltham, Massachusetts 02154

NiCd BATTERY ELECTRODES

C - 150

Second Quarterly Report

by

G. Holleck
M. Turchan
J. Hopkins

APR 1972
RECEIVED
NASA STI FACILITY
INPUT BRANCH

Contract No. 953185-NAS7-100

January 1972

NiCd BATTERY ELECTRODES
C - 150

Second Quarterly Report

by

G. Holleck
M. Turchan
J. Hopkins

Contract No. 953185-NAS7-100

January 1972

ABSTRACT

The objective of this research program is to develop and evaluate electrodes for a nongassing negative limited nickel-cadmium cell. The key element is the development of cadmium electrodes with high hydrogen overvoltage. For this, the following electrode structures were manufactured and their physical and electro-chemical characteristics were evaluated: (1) silver-sinter-based Cd electrodes, (2) Teflon-bonded Cd electrodes, (3) electrodeposited Cd sponge, and (4) Cd-sinter structures.

Silver-sinter-based Cd electrodes were prepared by the chemical impregnation method from silver-sinter plaques of high porosity. The developed plaques covered a wide variety of different structures with respect to both pore size and pore size distribution. The initial utilization of active material depended on the plaque type. In all cases, however, the capacity decreased with increasing cycle number. The rate of this capacity decrease was remarkably independent of plaque structure. It was considerably higher than with nickel-based Cd electrodes tested under the same conditions. Scanning electron micrographs of cycled electrodes showed the presence of needle-shaped crystals in silver-sinter-based Cd electrodes which could not be detected in nickel-sinter-based electrodes. To establish the significance of this difference would require further investigation. It appeared, however, that the use of silver as the plaque material in addition to plaque structure may have contributed to the electrochemical behavior of these silver-sinter-based Cd electrodes.

Electrodeposited Cd sponges were briefly investigated during this report period. In addition, a thorough investigation of Teflon-bonded Cd electrodes was initiated. Teflon-bonded Cd appears to represent a suitable electrode structure and is under further investigation.

iii

Porous cadmium structures were prepared from sodium fluoride compacts in the presence and absence of an inorganic flux. The electrochemical behavior is characterized by a high capacity and a sharp increase in potential at the end of charge with the advent of hydrogen evolution occurring at approximately -1.3 V versus Hg/HgO.

Table of Contents

List of Tables

List of Tables (Cont)

List of Illustrations

ix

List of Illustrations (Cont)

I. INTRODUCTION

The objective of this research program is to develop and evaluate electrodes for a nongassing negative limited nickel-cadmium cell. The concept of the negative limited cell and its implications on electrode structure were discussed in the First Quarterly Report.[1] The concept is based on the elimination of low hydrogen overvoltage materials from the negative plate. The onset of hydrogen evolution is then marked by a sharp increase in cell voltage, i.e., a signal that can be used to terminate the charging process.

Silver appears to be a suitable plaque material for high hydrogen overvoltage plate material as an alternative to pure cadmium structures. We measured the overvoltage for hydrogen evolution in 25% KOH on silver to be only approximately 100 mV more anodic than on cadmium and, we therefore, proposed to investigate a variety of fabrication techniques and to examine the electrochemical behavior of the following structures for use as negative plates:

1. Silver sinter on silver screen
2. Teflon-bonded cadmium hydroxide on silver screen
3. Cadmium sinter on silver screen
4. Cadmium sinter on cadmium screen
5. Teflon-bonded cadmium hydroxide on cadmium screen
6. Electrodeposited porous cadmium sponge on silver or cadmium screen.

Previously,[1] we reported on the manufacture of Teflon-bonded and silver-sinter-based Cd electrodes and on a preliminary evaluation of their physical and electrochemical characteristics. Both electrode structures exhibited a fairly sharp potential rise at the end of the charging cycle and the advent of gas evolution occurred at potentials between -1.2 and -1.3 V versus an Hg/HgO reference electrode at room temperature. With conventional nickel-sinter-based Cd electrodes, the advent of

hydrogen evolution occurred at approximately -1V versus the same reference electrode.

During this report period, we continued to study silver-sinter-based and Teflon-bonded Cd electrodes. We further investigated the feasibility of Cd sinter structures and electrodeposited porous cadmium sponge for use as negative plates in a negative limited, sealed NiCd battery.

II. DEVELOPMENT OF NEGATIVE ELECTRODE STRUCTURES

A. Silver-Sinter-Based Cd Electrodes

1. Silver sinter structures

A large variety of different silver sinter structures with high porosities was prepared. This was achieved by utilizing a variety of silver powders and by using different preparation techniques such as the sintering of loose powder layups and of sodium fluoride compacts. The latter requires, as a final step, the removal of the inert filler by a leaching process. Detailed experimental procedures were reported previously.[1] In the following discussion, the structures, coded according to the silver powder used, are investigated more closely by means of scanning electron microscope photographs of the powder and of the sintered plaques. Cross sections were obtained by fracturing the plaques in liquid nitrogen. The macroscopic characteristics of Silpowder "130", "150", and "220" (such as apparent density, Fischer average particle diameter, etc.) were included in the previous quarterly report.

a. Plaque type "150": Silpowder "150" is shown in Figs. 1 and 2. It consisted of relatively large agglomerates of individual particles. Both the agglomerates and the individual particles exhibited a wide range of differing sizes. Plaques obtained by sintering (30 min at 550°C) of dry layups of this powder retained these characteristics (Figs. 3 and 4). They exhibited a very pronounced double porosity. Large pores were formed between the individual agglomerates which themselves remain porous. They showed, however, considerable necking by interdiffusion. The macroscopic porosity was approximately 75%.

b. Plaque type "130": Silpowder "130" (Figs. 5 and 6) showed a very small average particle size, and a nearly spherical shape. It too contained particles with a wide variation in size. This powder had poor flow characteristics and exhibited a tendency to agglomerate. These agglomerates had, however, no
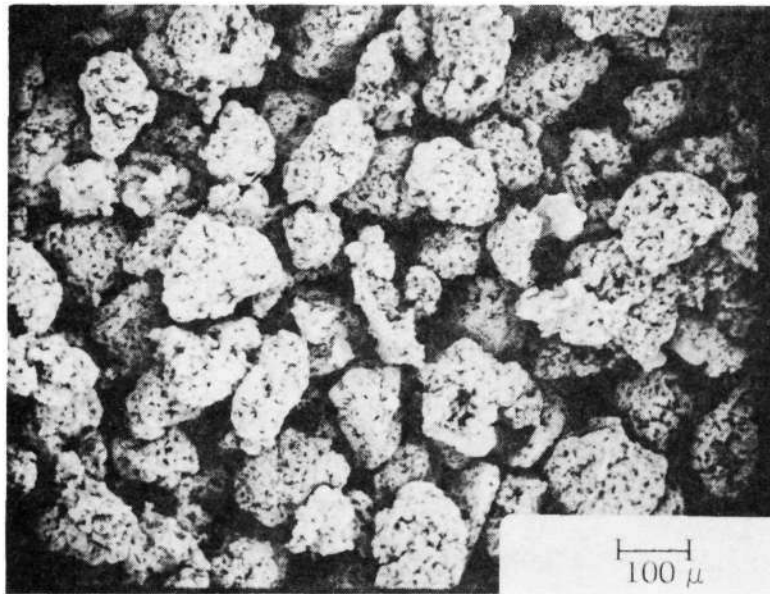
Fig. 1. Silverpowder, Handy and Harman 150

Fig. 2. Silverpowder, Handy and Harman 150
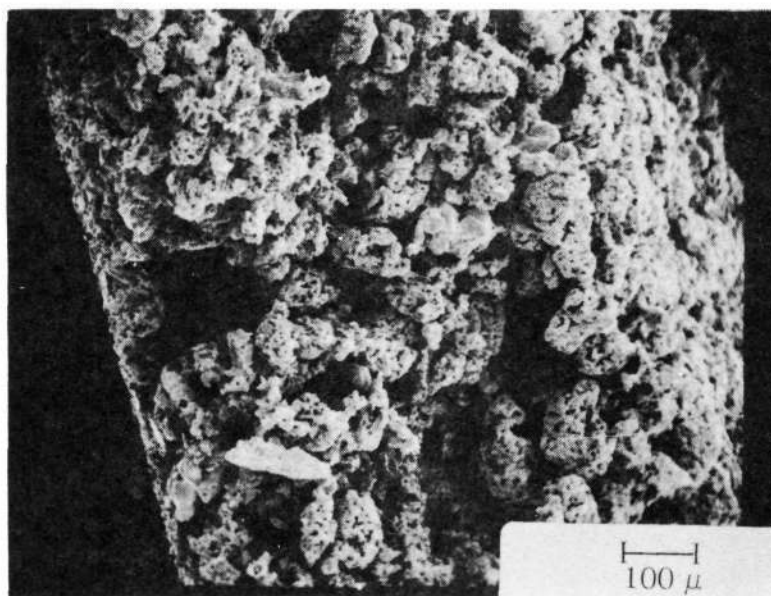
Fig. 3. Silver-sinter plaque 150
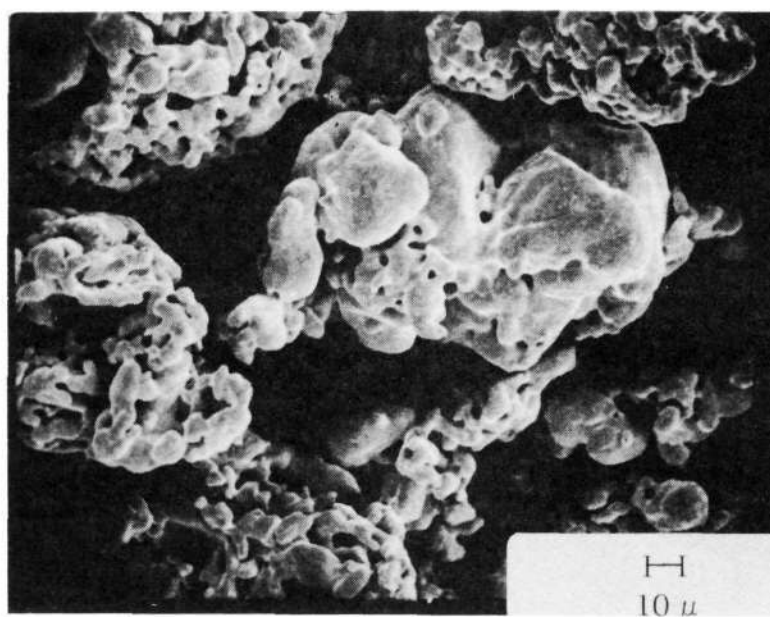
Fig. 4. Silver-sinter plaque 150

Fig. 5. Silverpowder, Handy and Harman 130
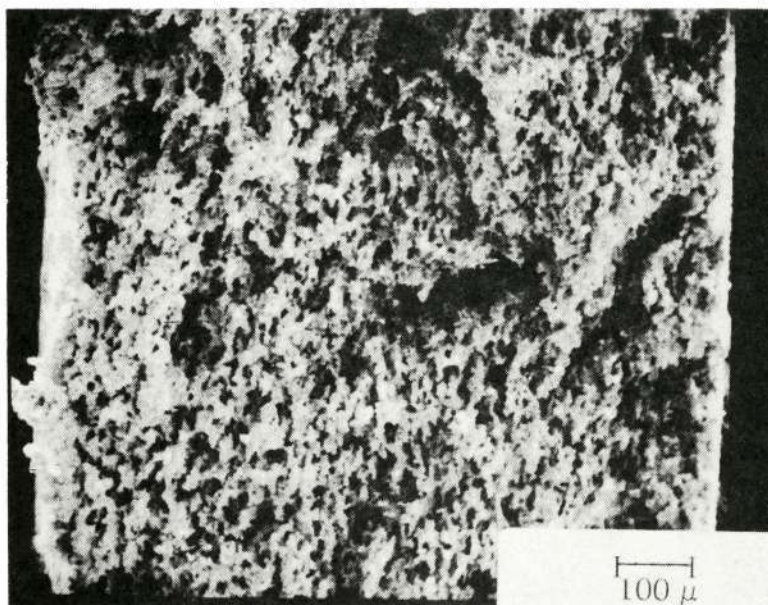
Fig. 6. Silver-sinter plaque 130 (NaF compact)

characteristic size or shape as opposed to Silpowder "150". A typical plaque obtained by sintering and leaching of a NaF compact (60 vol % NaF, 25,000 psi, 30 min at 600°C) is shown in Figs. 6 and 7. The pore size distribution was much more uniform than in the "150" plaque. The cross section in Fig. 6 also showed a directional orientation of the silver agglomerates introduced by the pressing of the compact.

c. Plaque type "220": Fig. 8 shows Silpowder "220". These particles had an irregular, elongated shape and the particle size distribution was much more uniform than the previously mentioned silver powders. The macroscopic flow characteristics of the Ag powder were quite good. The powder contained some agglomerates although without characteristic size or shape. A fractured cross section of a sintered "220" powder layup is shown in Fig. 9. It appeared as a double structure with larger and smaller pores. The shape of the pores and the necking between the particles is illustrated in Fig. 10.

Modified "220" type plaque structures were obtained by: (1) mixing 10% silver oxide (Fisher purified Ag_2O, lot no. 742450) with the Ag powder before making the dry layup, and (2) by vacuum impregnating a "220" plaque with a saturated $AgNO_3$ solution followed by decomposition to Ag at 450°C. The reasoning behind these modifications was to increase the internal surface area of these structures. The results of both methods were quite similar. Fig. 11 shows a Ag_2O modified structure. It was very similar to the regular "220" plaque except for the presence of small dimples on the internal surface.

A different plaque structure was obtained by sintering and leaching a sodium fluoride compact. Fig. 12 clearly shows the structural orientation parallel to the surface. The surface also had a distinctly different appearance (Fig. 13). Here we see relatively large flat areas with only small pores, whereas the surface appearance of sintered dry layups is very similar to cross sections of such structures.

d. Plaque type "300": The Silpowder "300" is shown in Figs. 14 and 15. It exhibited a double structure similar to Silpowder "150" and consisted of agglomerates of various size made up of small dendritic particles (Fig. 15). Sinters produced from this powder also showed a dual porosity range. Fig. 16 shows the sintered structure to be much finer than in the previously discussed plaques. It retained many features of the dendritic powder. The mechanical stability of the type "300" plaque was poorer compared to the other plaques. An increase of the sintering time from 30 min (at 550°C) to 60 min slightly improved the mechanical stability without noticeable changes in plaque structure.
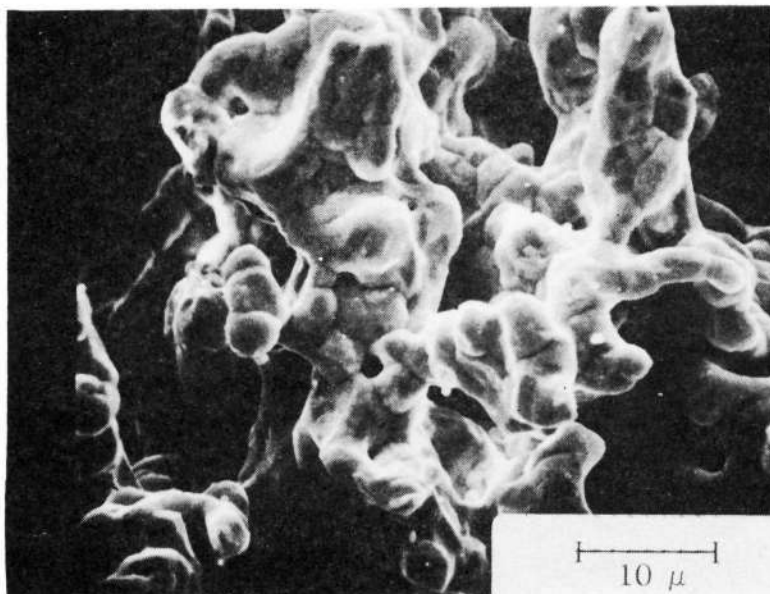
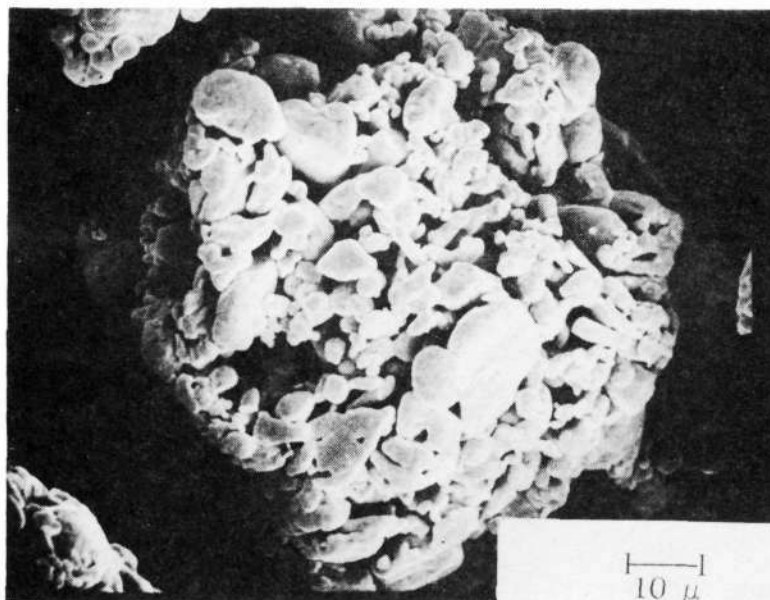Fig. 7. Silver-sinter plaque 130 (NaF compact)
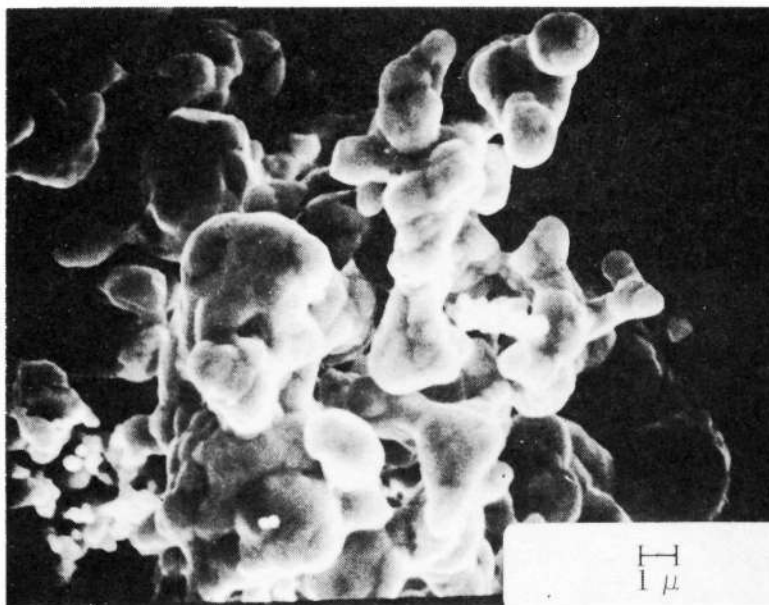
Fig. 8. Silverpowder, Handy and Harman 220
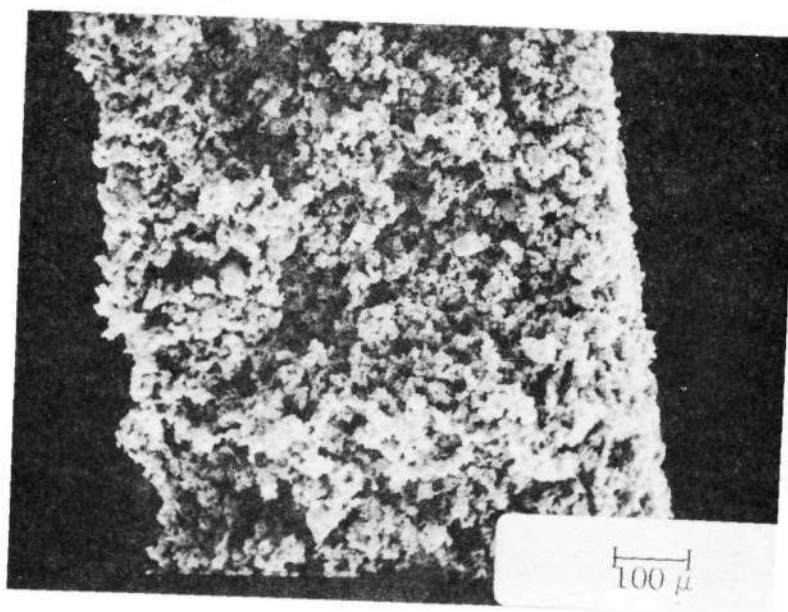
Fig. 9. Silver-sinter plaque 220
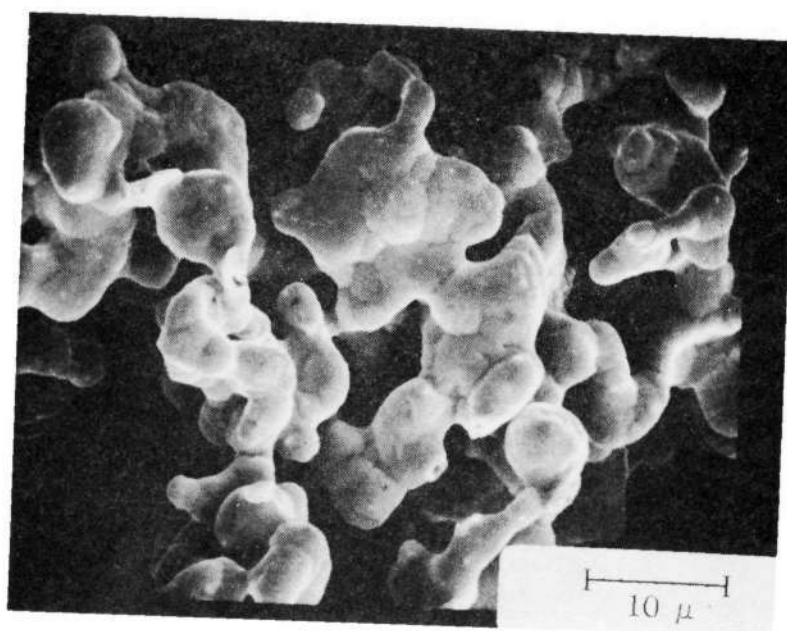
Fig. 10. Silver-sinter plaque 220
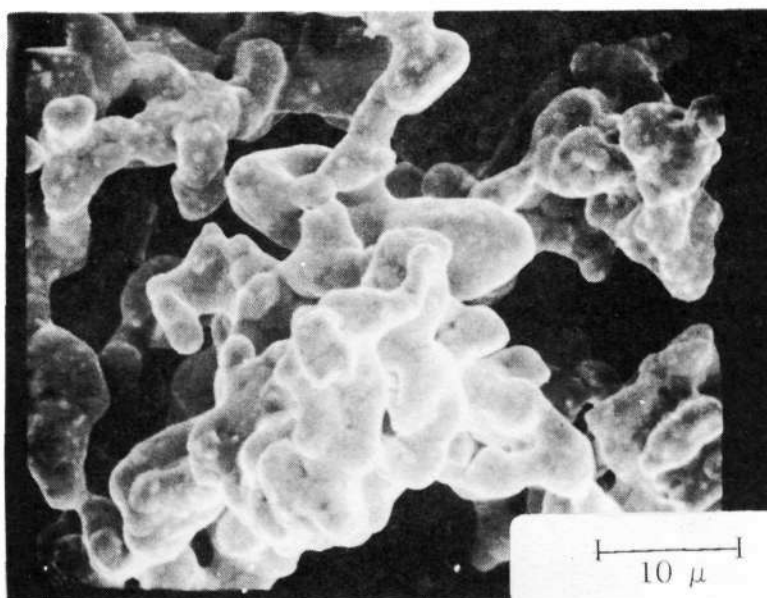
Fig. 11. Silver-sinter plaque 220 (Ag$_2$O modified)
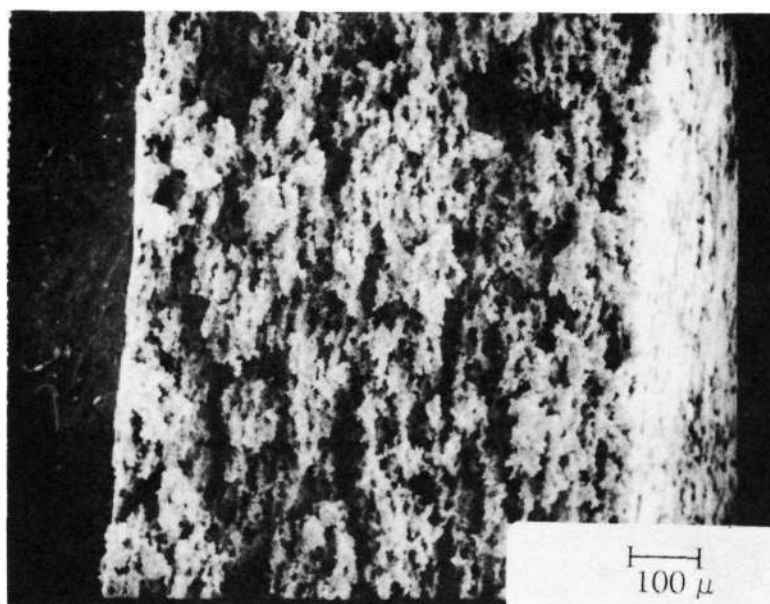
Fig. 12. Silver-sinter plaque 220 (NaF compact)
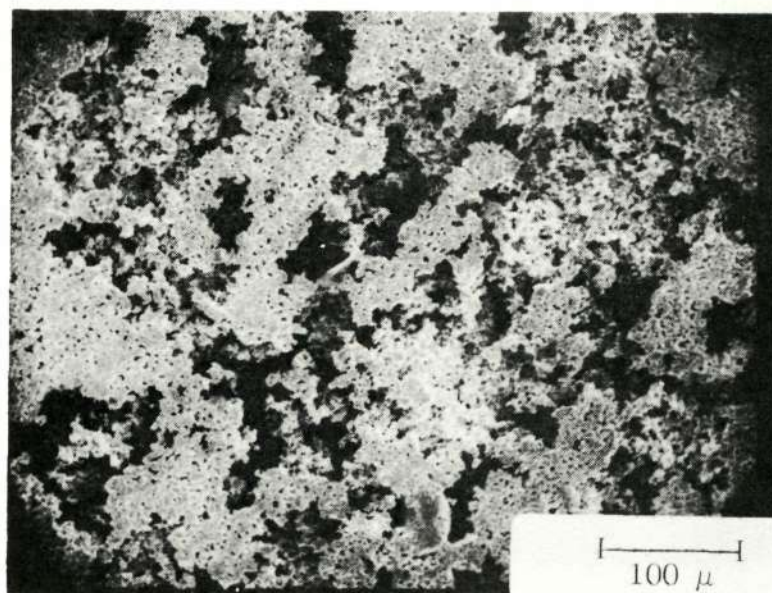
Fig. 13. Silver-sinter plaque 220 surface (NaF compact)
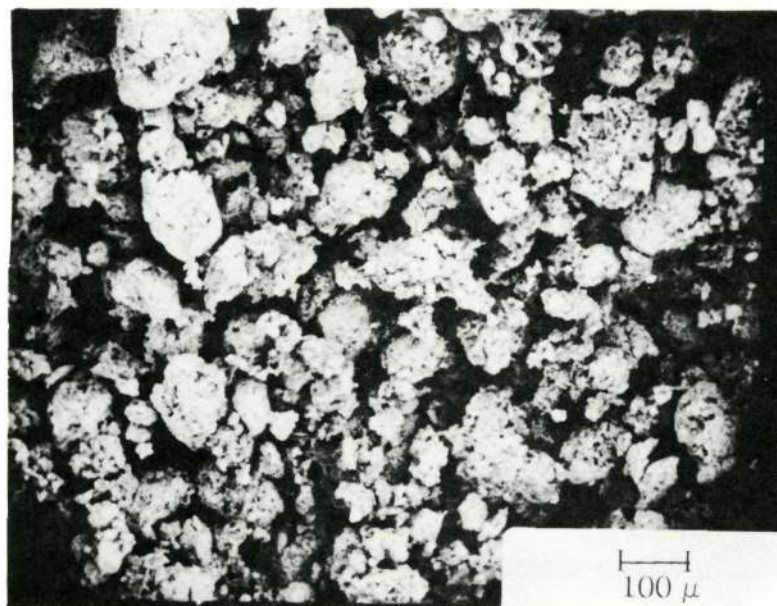
Fig. 14. Silverpowder, Handy and Harman 300

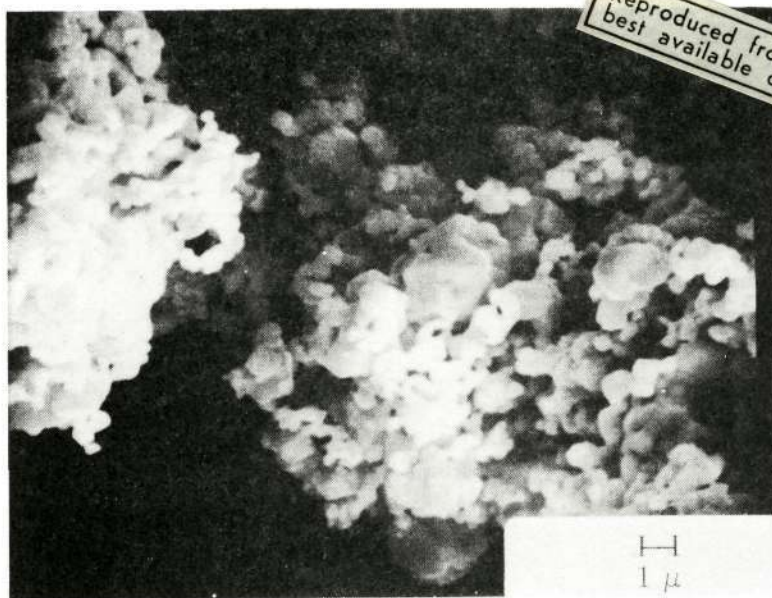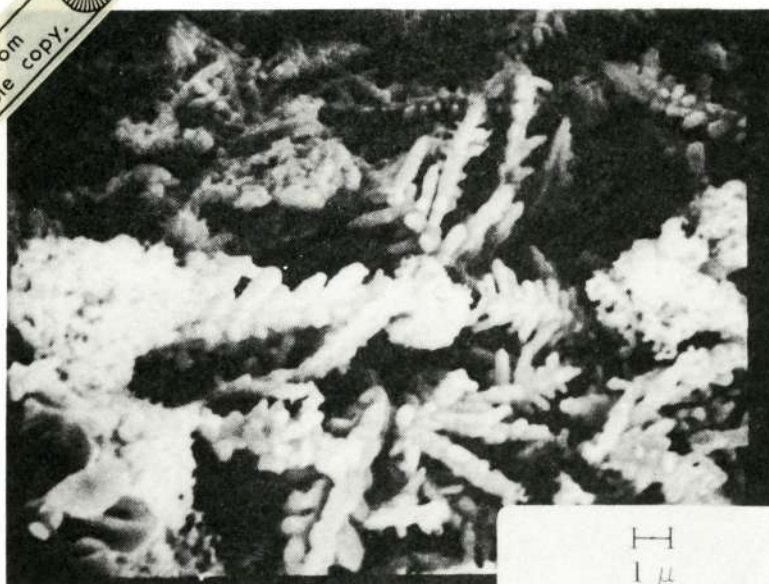Fig. 15. Silverpowder, Handy and Harman 300
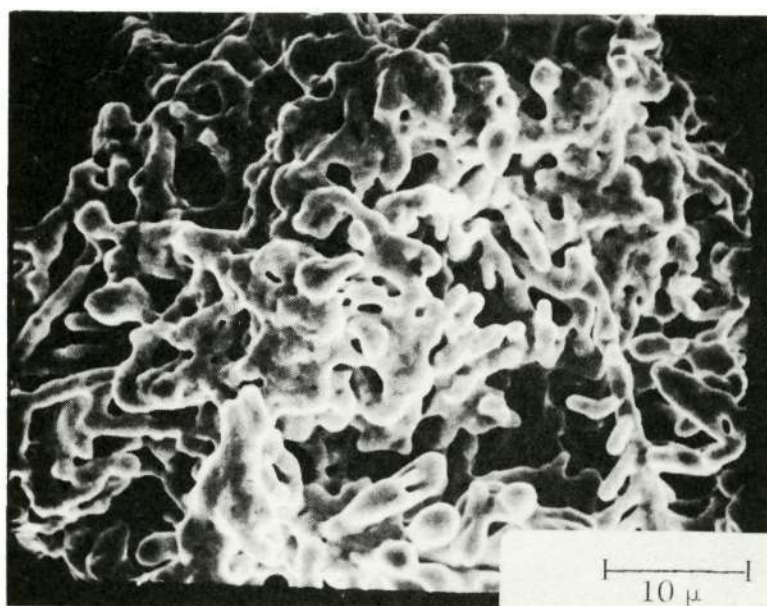
Fig. 16. Silver-sinter plaque 300

- 12 -

For purposes of comparison, Fig. 17 shows the structure of a commercial nickel plaque. The pore size distribution seemed to be somewhat more uniform than in most silver sinter plaques; however, we found a number of large pores. With regard to average pore size, the nickel sinters would have to be placed between the type "300" silver plaque and the remaining types of silver sinter structures.

2. Electrochemical evaluation of silver sinter structures

The various silver sinter structures discussed above were impregnated with cadmium hydroxide by the chemical conversion method, i.e., vacuum impregnated with saturated CdNO$_3$, dried, then chemically converted in KOH at 80°C. The plaque characteristics and the loading of these cadmium electrodes are summarized in Table I. The charge and discharge voltage profiles of the various silver-sinter-based Cd electrodes were very similar. Characteristic examples are shown in Figs. 18 to 20. The charge and discharge plateaus were quite flat and the advent of gas evolution as characterized by the initial appearance of small individual gas bubbles at the electrode surface, occurred at approximately -1.25 V versus Hg/HgO.

The capacity of the various electrodes (stated as per cent of their theoretical capacity) as a function of the number of cycles is summarized in Table II. Table II will serve as the basis for the following comparative discussion of electrode behavior, even though individual capacity values of the different electrodes may not be exactly comparable due to variations in operating conditions such as current density and cutoff voltages. Significant changes during the cycling are indicated in the Table. More detailed information on the test behavior of each individual electrode is given in the Appendix.

An important feature common to all silver-based electrode structures was the rapid decrease in capacity with increasing number of cycles. The rate of decrease was somewhat accentuated by cycling the electrodes at a constant current density which results in an increasing charge and discharge rate as the electrode capacity decreases. Generally, a decrease in current density, a cathodic shift of the charge cutoff voltage or charging into hydrogen evolution increased electrode capacity. After this initial increase, however, the capacity continued to decrease as before. This behavior is best illustrated in Table II by electrodes SS Cd-1, 2, 4 and 6. Potentio-stating the electrode at -1.2 V versus Hg/HgO overnight (H$_2$ evolution < 0.1 cc) also restored part of the "lost" capacity.

The initial utilization of active material varied with the different electrode structures. For example, plates of type "220" showed an initial utilization of approxi-
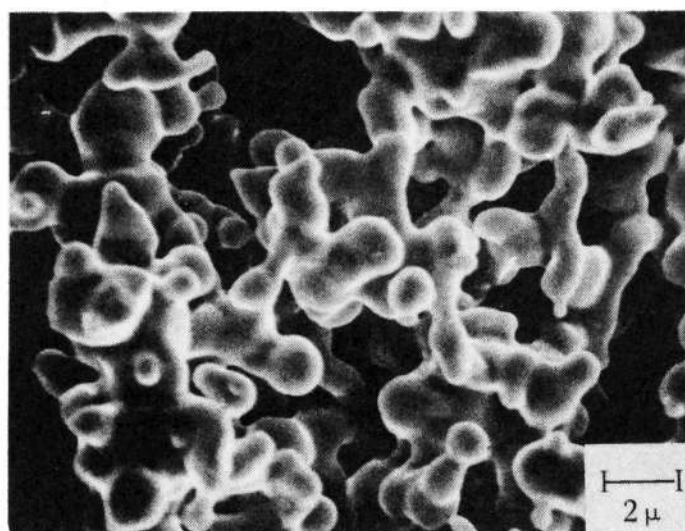
Fig. 17. Commercial nickel plaque

Table I. Characteristics of Silver-Sinter-Based Cd Electrodes

Electrode	Plaque Type	Plaque Porosity, %	Plate Thickness, mil	Theoretical Capacity	
				Ahr	Ahr/in.^{3}
SS Cd-1	Ag 150 dry layup (sample)	74	30	0.364	8.1
SS Cd-2	Ag 130 NaF compact	71	39	0.248	6.3
SS Cd-3	Ag 220 dry layup	77	28	0.218	7.9
SS Cd-4	Ag 130 dry layup	76	25	0.160	6.6
SS Cd-5	Ag 150 dry layup (batch)	72	32	0.223	5.2
SS Cd-6	Ag 220 dry layup	77	24.5	0.133	3.6
SS Cd-7	Ag 220 dry layup	78	25	0.134	3.7
SS Cd-8	Ag 220 dry layup (AgNO$_3$ modified)	81	19	0.142	4.9
SS Cd-9	Ag 220 dry layup (AgNo$_3$ modified)	81	19	0.139	5.1
SS Cd-10	Ag 220 dry layup (Ag$_2$O modified)	78	21	0.106	4.9
SS Cd-11	Ag 300 dry layup	82	21	0.162	5.3
SS Cd-12	Ag 300 dry layup	82	21	0.124	4.8
SS Cd-13	Ag 300 dry layup	82	21	0.146	4.9
NS Cd-3	Ni 287 dry layup	76	35	0.325	12.2
NS Cd-4	Ni 287 dry layup	76	35	0.650	12.2
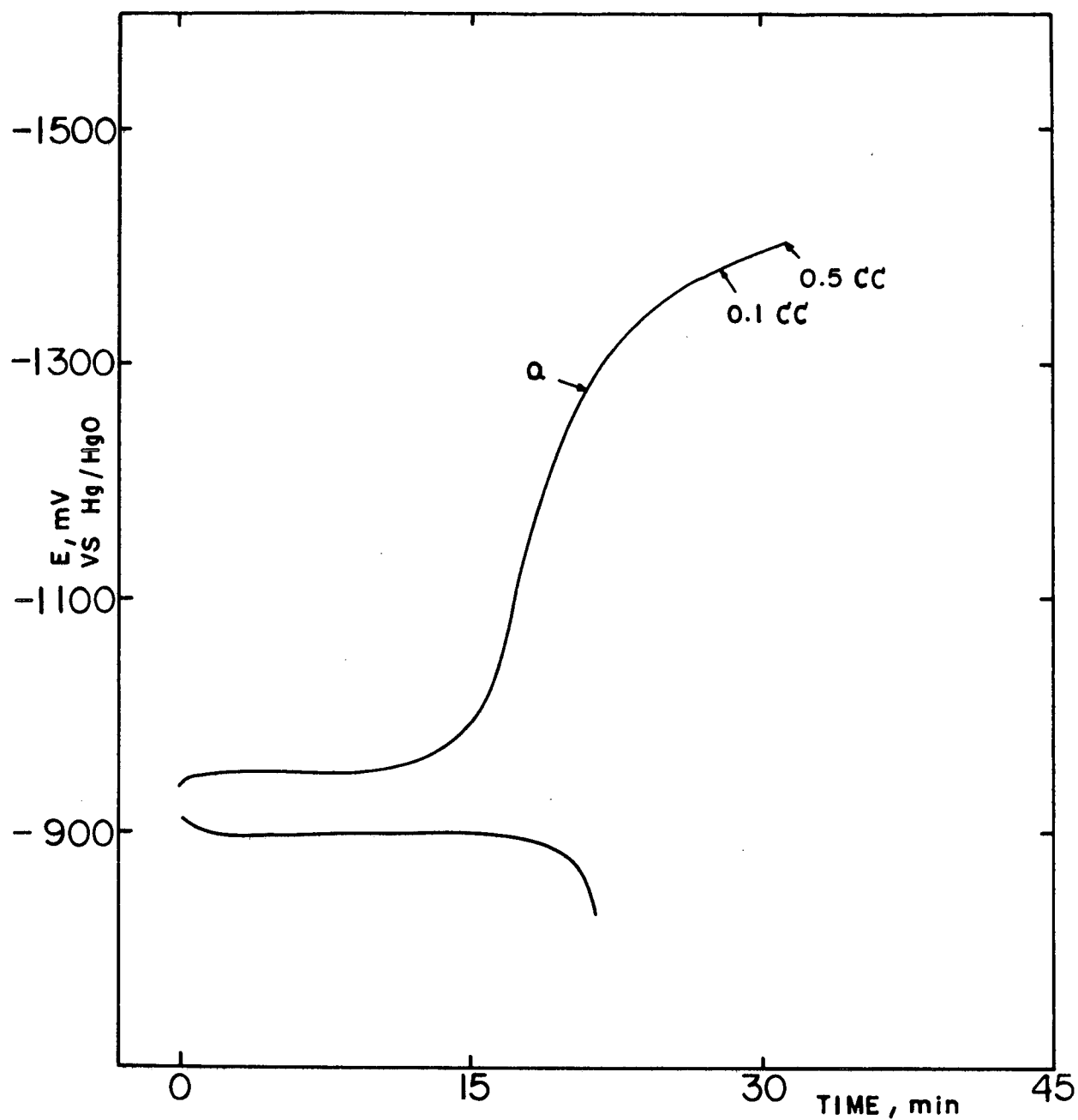
Fig. 18. Charge and discharge cycle of silver-sinter-based Cd electrode
SS Cd-2 (Ag 130, NaF compact, cycle no. 32, 7 mA/cm^2, 25% KOH,
room temperature; a = first individual, small bubbles)
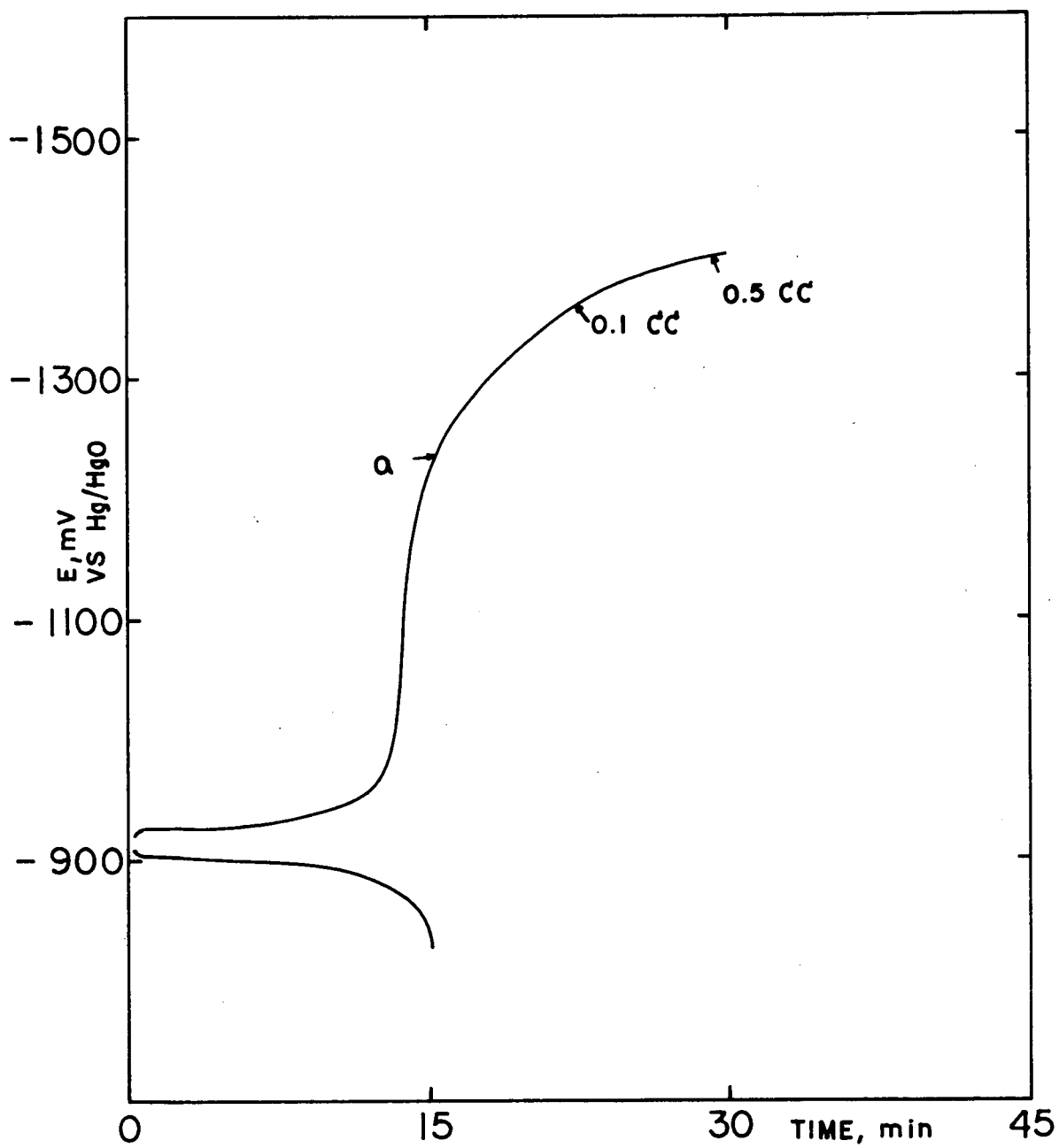
Fig. 19. Charge and discharge cycles of silver-sinter-based Cd electrode
SS Cd-3 (Ag 220, cycle no. 40, 7 mA/cm^2, 25% KOH, room
temperature; a = first individual, small bubbles)
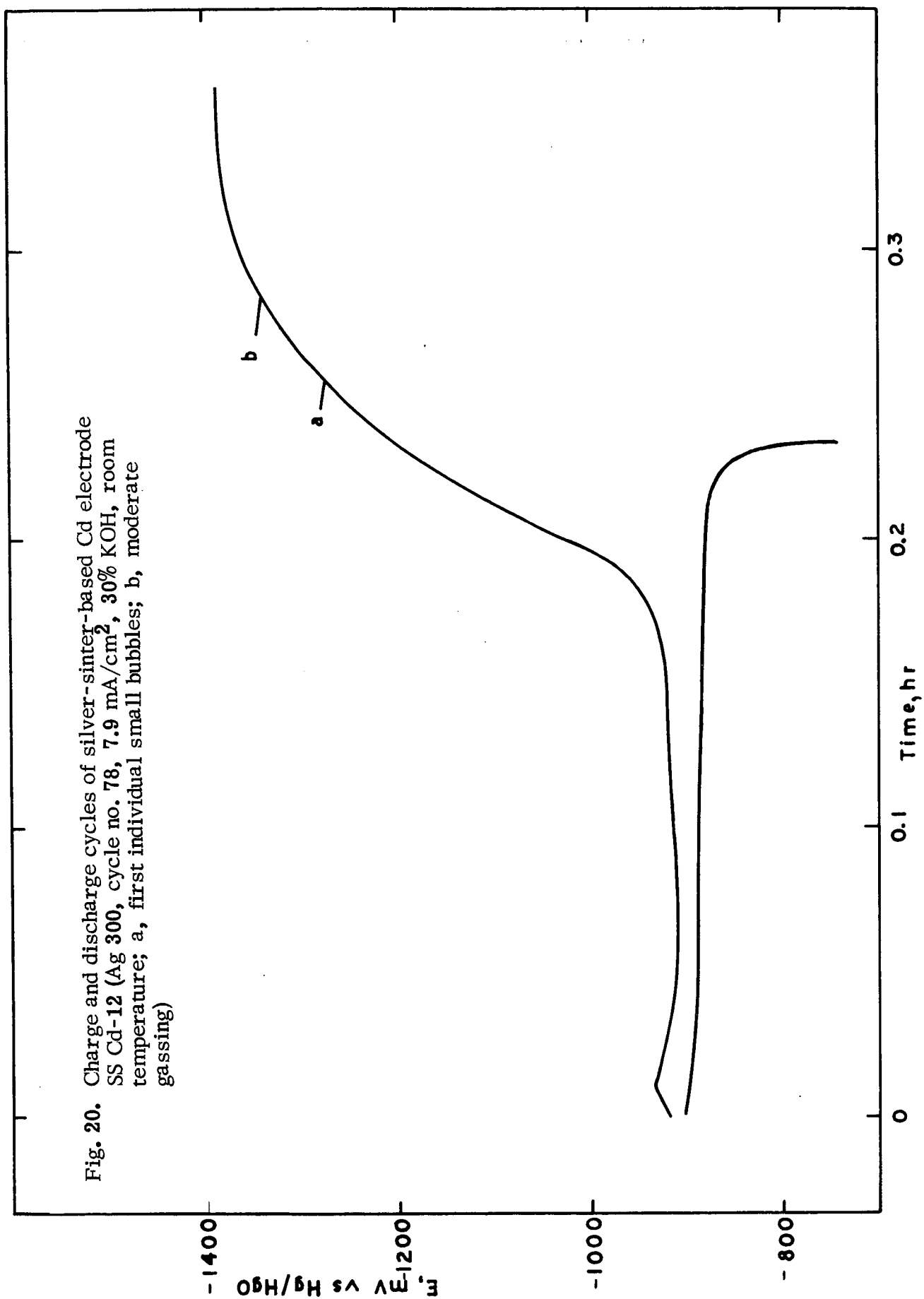
Fig. 20. Charge and discharge cycles of silver-sinter-based Cd electrode SS Cd-12 (Ag 300, cycle no. 78, 7.9 mA/cm^2, 30% KOH, room temperature; a, first individual small bubbles; b, moderate gassing)

- 18 -

Table II. Capacity of Silver-Sinter-Based Cd Electrodes
(Measured Capacity as Percent of Theoretical Capacity)

SS Cd-	1	2	3	4	5	6	7	8	9	10	11	12	13
Ag Powder Cycle No.	150	130C	220	130	150	220	220	220 mod.	220 mod.	220 mod.	300	300	300
1	70.0	42.0	54	42.5	49.3	28.5	38.8	74.6	67.6	74.5	72.0	74.5	70.0
5	46.2	21.0 †	29.0	27.5	33.2	18.8 †	26.8 †	53.5	50.4	53.7	44.5	48.8	45.5
10	34.5	13.0	21.0	20.0	22.4	19.5	22.0	38.0	40.3	40.5	30.8	34.2	31.5
20	23.8 *	9.0 †	15.5 *	12.5	13.7	9.8	11.2	23.2	26.6	25.4	18.5	22.6	18.5
30	18.3 *	7.0 *	12.0	8.1	9.5	7.1	8.4 †	18.3	20.9	20.3	16.3	16.5	14.0
40	25.1	13.0	8.0	7.0 **	7.2	6.0 †	6.7	15.5	17.7	16.5	11.4	14.1	11.6
50	15.3	4.2	-	20.0	6.3 **	5.4	4.5	13.4	14.0 †	14.1 †	9.9	12.1	11.0
60	11.2	2.6	-	15.0	17.9	4.7	-	12.3	14.0	16.5	9.0	10.9	8.9
Charge discharge rate limits	0.5-1	1-10	1-3	1.5-10	1-5	1.5-5	2-4	0.5-4	0.5-2	0.7-3	0.5-4	0.5-4	0.5-4

* Charged into H_2 evolution or potentiostated.

** Charge cut off shifted more cathodic.

† Current density reduced.

- 19 -

mately 40 to 50% of the theoretical capacity. The modification of these structures by the use of $AgNO_3$ and Ag_2O resulted in a roughening of the internal surfaces increasing the initial utilization to approximately 75% of the theoretical value. The very fine structures of type "300" also exhibited a high initial utilization.

The rate of decrease of electrode capacity as a function of the number of cycles was, however, remarably similar for the wide variety of plaque structures. This is graphically illustrated in Figs. 21 and 22. Generally, the electrodes lost under these conditions approximately half of their capacity after 5 to 10 cycles and this value was again cut in half at approximately 20 to 30 cycles. A closer analysis of the cycling data showed that the capacity loss did not appear to be confined to either the charge or the discharge cycle. As Table III shows, the capacity between two preset potential values changed continuously from charge to discharge and following charge, etc.

In order to obtain a reliable basis for comparison of silver-sinter-based Cd electrodes with conventional nickel-sinter Cd electrodes, we subjected the latter to the same test conditions. The upper voltage cutoff was set to approximately -1 V versus Hg/HgO to avoid H_2 evolution. The results are shown in Table IV, V, and VI. NS Cd-2 is a commercial nickel-sinter-based Cd electrode. Its original plate characteristics and the previous cycling history were unknown. The pertinent data for NS Cd-3 and NS Cd-4 are included in Table I. In anology to some early testing of silver-sinter-based electrodes, NS Cd-3 was not subjected to any prior formation cycling. Except for the first few cycles, these nickel-sinter-based Cd electrodes showed only a very small change in capacity upon cycling. For example, the capacity of NS Cd-3 changed between cycle 25 to 225 only from 38.8% to 34% of its theoretical capacity.

To obtain further information which could explain the unexpected behavior of silver-sinter-based Cd electrodes, we investigated the morphology of cycled structures by scanning electron microscopy. Figs. 23 to 28 show scanning electron microscope cross section of various cycled electrodes. Especially noteworthy are the needle shaped crystals in the cycled electrodes SS Cd-4 and SS Cd-5 (Figs. 23 and 24). Fig. 25 shows a "220" type plaque after three cycles. There were few larger crystals in this structure. The internal silver surface was quite uniformly covered by a very fine crystalline mass. Cycled electrode SS Cd-8 is shown in Fig. 26. Large, regularly shaped crystals located throughout the sinter structure with no apparent needles were observed. In electrode SS Cd-12, the large regularly shaped crystals could be seen more clearly. It should be noted that cycling of this electrode was interrupted in the

Fig. 21. Capacity change of-Cd impregnated silver sinters [a, types 130 and 220; b, type 150; c, type 300; d, type 220 modified (room temperature 25% KOH)]

Fig. 22. Capacity change of Cd-impregnated silver sinters (room temperature)
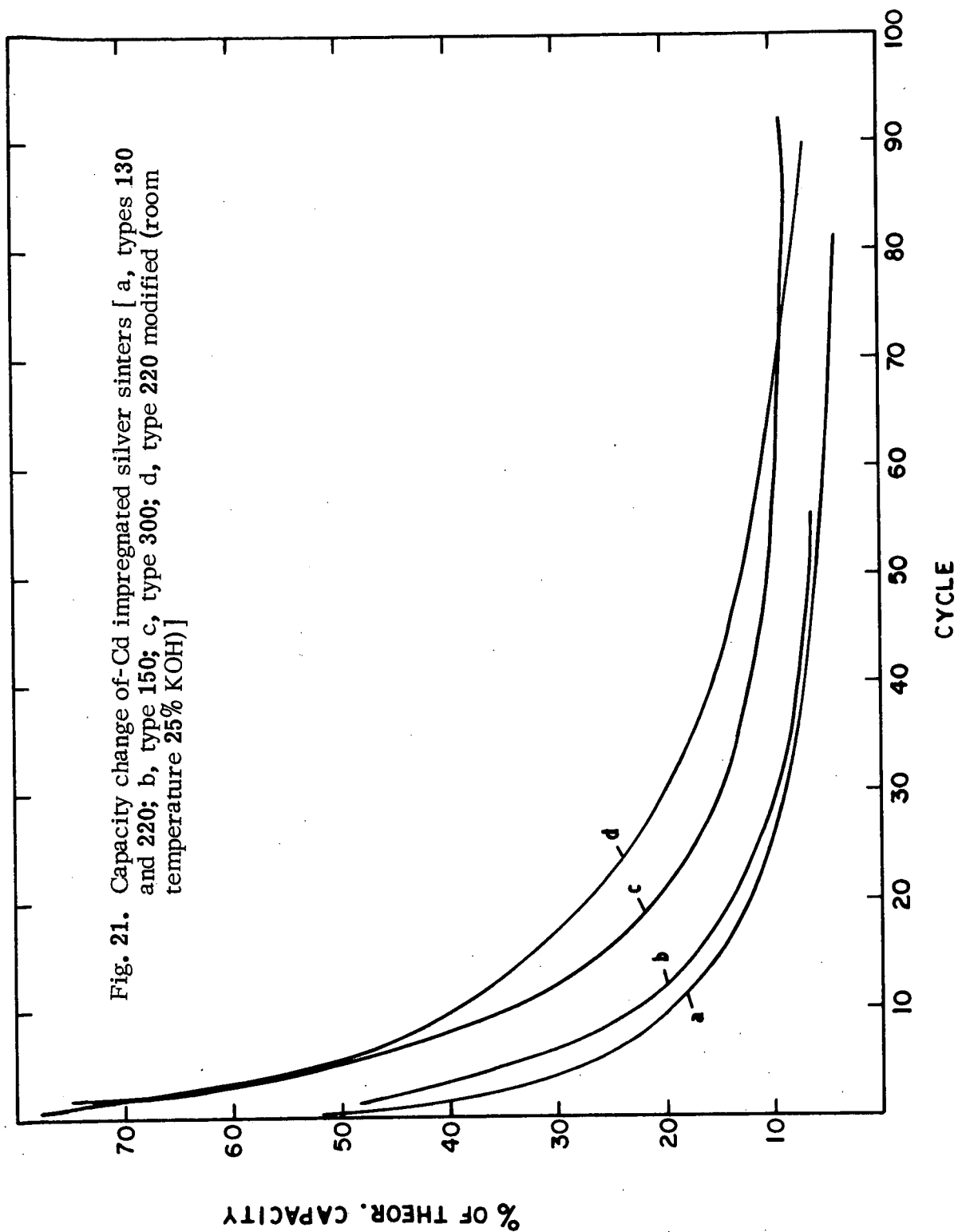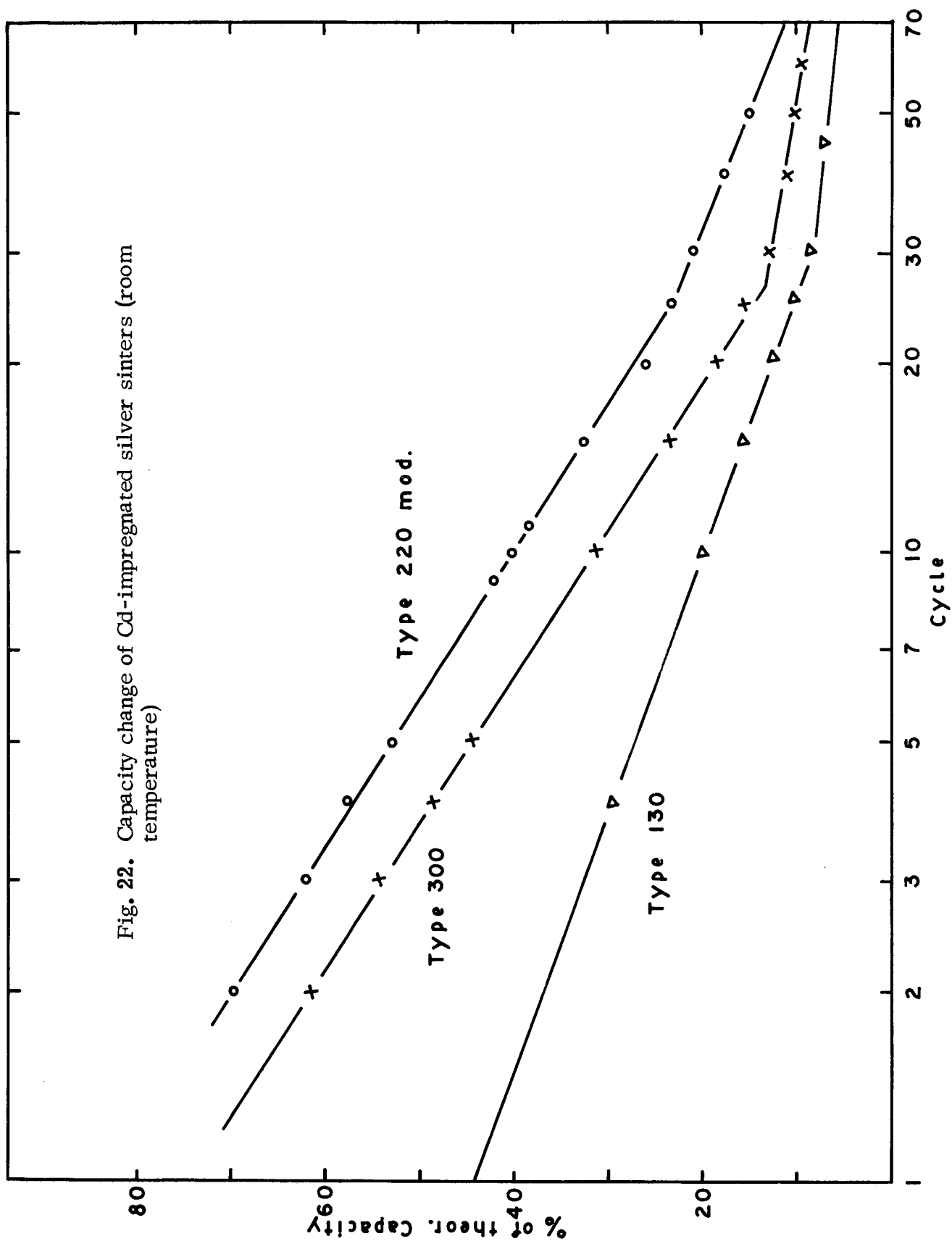
Table III. Charge and Discharge Times Between Preset Voltage Limits at Constant Current Density

Cycle No.	SS Cd-2		SS Cd-3	
	Charge, hr	Discharge, hr	Charge, hr	Discharge, hr
1	1.25	0.88	1.5ψ	1.18
2	0.83	0.68	1.05	0.90
3	0.64	0.56	0.82	0.75
4	0.52	0.49	0.72	0.67
5	0.47	0.42	0.65	0.62
10	0.30	0.28	0.47	0.45
11	0.28	0.26	0.45	0.43
12	0.27	0.25	0.42	0.41

Table IV. Commercial Ni Plaque Cd Electrode NS Cd-2
(Room Temperature, 25% KOH)

No. of Cycles	Discharge, hr	Capacity, Ahr	Comments
3	3.44	0.344	10 mA/cm^2; cycled -775 to -1075 mV vs Hg/HgO; some H$_2$ evolution
5	3.54	0.354	
9	3.75	0.375	
10	1.85	0.370	20 mA/cm^2; cycled to -800 to -1050 mV vs Hg/HgO
15	1.78	0.356	
20	1.88	0.376	
25	1.88	0.376	
30	1.86	0.372	
35	1.86	0.372	
40	1.90	0.380	
50	1.87	0.374	
73	1.75	0.350	

Table V. Ni Plaque Cd Electrode NS Cd-3 (Room Temperature, 25% KOH, No Prior Formation)

No. of Cycles	Discharge, hr	Capacity, % of Theoretical	Comments
1	1.7	52.3	15.5 mA/cm^2; cycled -725 to -960 mV vs Hg/HgO; no H$_2$ evolution
2	1.65	50.8	
5	1.20	39.4	
10	1.33	40.9	15.5 mA/cm^2; cycled -725 to -1025 mV vs Hg/HgO; negligible H$_2$ evolution
15	1.31	40.3	
18	1.43	44.0	
20	1.39	42.8	
25	0.63	38.8	31 mA/cm^2; cycled -750 to -1000 mV vs Hg/HgO; no H$_2$ evolution
30	0.63	38.8	
40	0.59	36.3	
50	0.62	38.2	
60	0.62	38.2	
75	0.59	36.3	
100	0.58	35.7	
125	0.60	37.0	
140	0.59	36.3	
225	0.55	34.0	

Table VI. Ni Plaque Cd Electrode NS Cd-4 (Room Temperature, 30% KOH, Formed)

No. of Cycles	Discharge, hr	Capacity, % of Theoretical	Comments
1	1.77	54.5	15 mA/cm^2; cycled -800 mV to -110 mV vs Hg/HgO
5	1.64	50.5	
10	1.60	49.2	
20	1.46	45.0	
30	1.42	43.8	
40	1.38	42.5	
50	1.34	41.3	
60	1.33	41.0	
70	1.30	40.0	
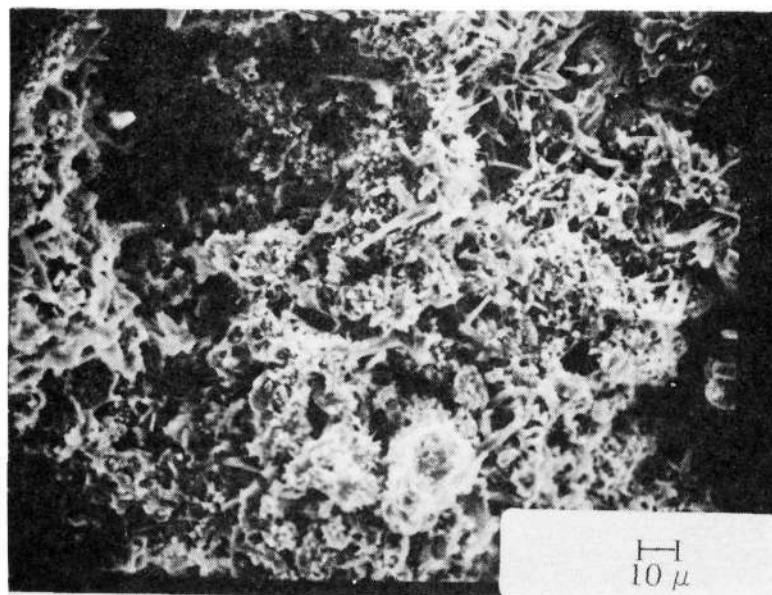
Fig. **23.** Cycled Cd-impregnated Ag sinter **130** (SS Cd-**4,** >**150** cycles, discharged)
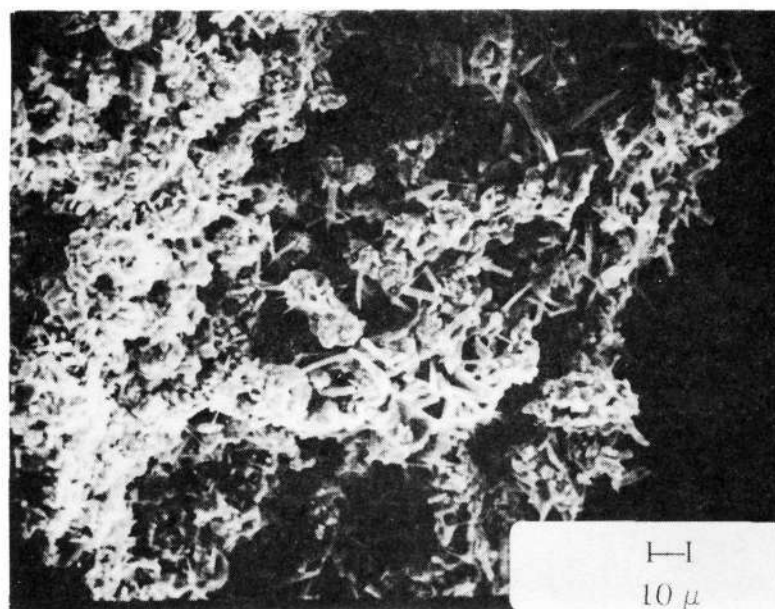
Fig. **24.** Cycled Cd-impregnated Ag sinter **150** (SS Cd-**5,** >**125** cycles, discharged)
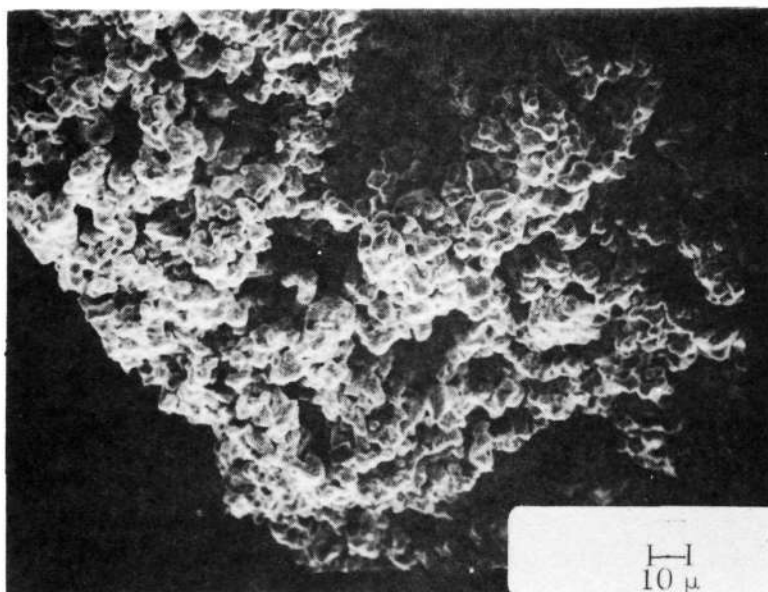
Fig. 25. Cycled Cd-impregnated Ag sinter 220 (three cycles, 80% discharged)
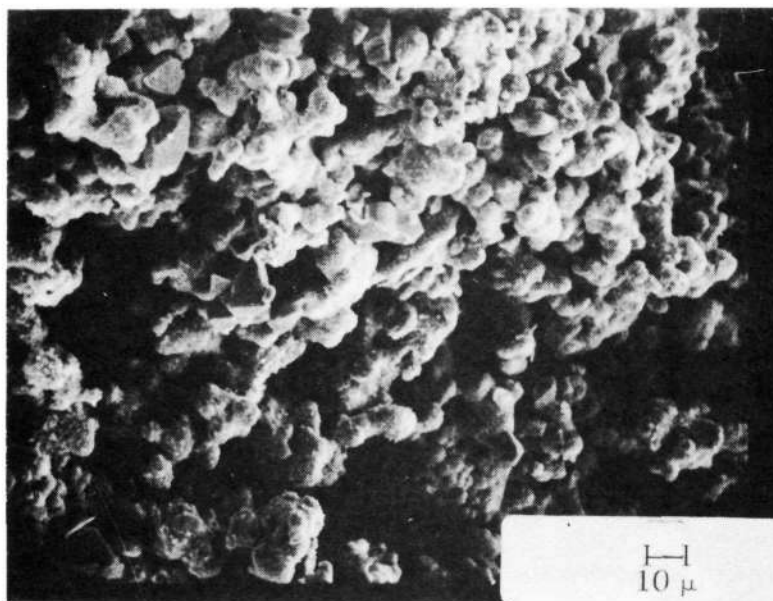
Fig. 26. Cycled Cd-impregnated Ag sinter 220, $AgNO_3$ modified (SS Cd-8, 133 cycles, 83% discharged)
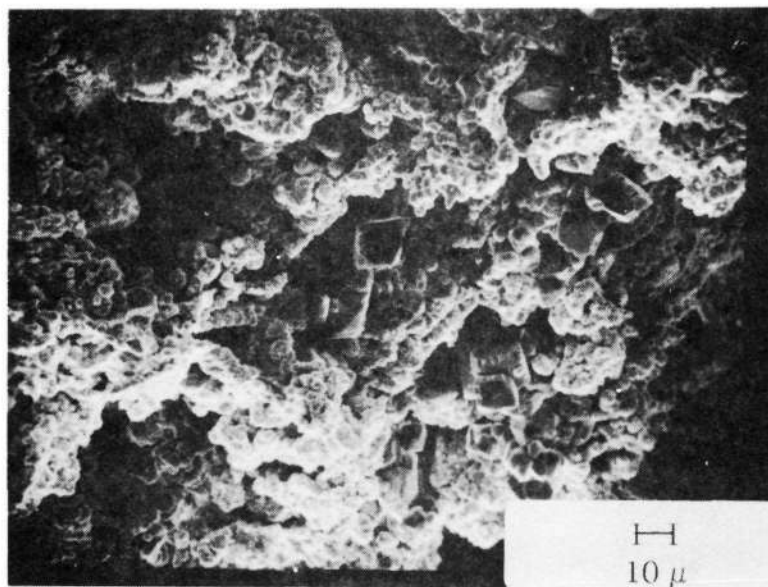
Fig. 27. Cycled Cd-impregnated Ag sinter 300 (SS Cd-12, 104 cycles, charged)
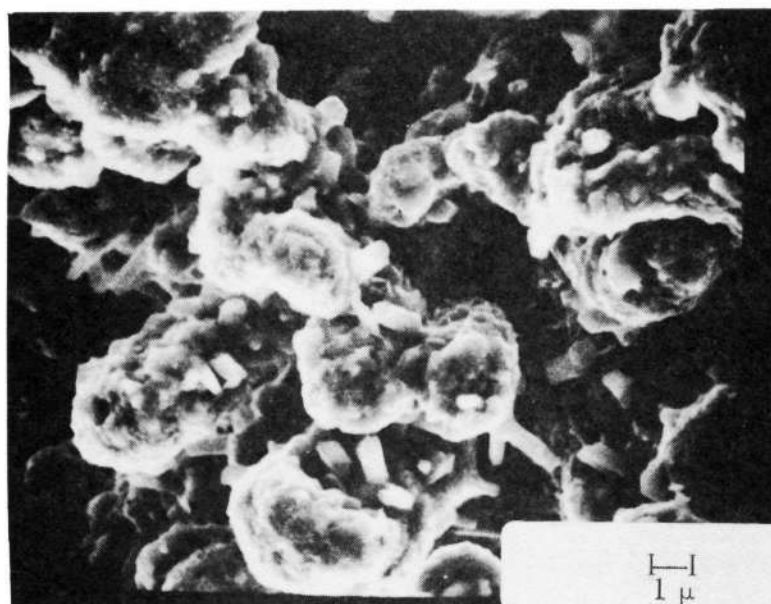
Fig. 28. Cycled Cd-impregnated Ag sinter 300 (SS Cd-12, 104 cycles, charged)

fully charged state. Even though needle-shaped crystals are not apparent in this photomicrograph, a higher magnification showed that they were present in this structure (Fig. 27).

For comparison, Fig. 29 shows a cycled nickel-sinter-based electrode (NS Cd-4). Crystalline and amorphous particles seem to be intermixed. No needle-shaped crystals were detectable.

3. Conclusions

The silver sinters investigated here covered a wide variety of different structures with respect to both pore size and pore size distribution. The initial utilization of active material depended on the plaque type. The rate of capacity decrease with the number of cycles was surprisingly independent of structure; it was considerably higher than with nickel-based Cd electrodes tested under the same conditions. Scanning electrode micrographs of cycled electrodes showed the presence of needle-shaped crystals in silver-sinter-based Cd electrodes which could not be detected in nickel-sinter-based electrodes. To establish the significance of this difference requires further investigation. It appeared, however, that the use of silver as the plaque material in addition to plaque structure may have been responsible for the electrochemical behavior of these silver-sinter-based Cd electrodes.

B. Teflon-Bonded Cadmium Electrodes

1. Electrode preparation

The composition of the Teflon-bonded electrode TFE-4 was equal to TFE-3 (78.2% CdO, 8.7% Teflon, 12.1% silver flake on 5 Ag7, 4/0 expanded silver). TFE-4 was prepared by sieving the dried powder mix into a mold. Midway through this procedure, the expanded silver screen was inserted. The mixture was pressed at 7.5 ton/in.^{2} for 5 min and sintered in an inert atmosphere for 20 min between 280 and 285°C. The final electrode was 24 mil thick.

The Teflon-bonded electrode TFE Cd-1 contained only cadmium. It was prepared by pasting a wet mixture of 87% $Cd(OH)_2$, 5% Cd powder (Cominco -200 mesh) and 8% Teflon on an expanded cadmium metal screen (10 Cd 10, 3/0). After drying, the electrode was sintered in a N_2 atmosphere at 250°C for 10 min. The final thickness of the electrode was 42 mil.

2. Electrochemical evaluation

Before cycling, the electrode was potentiostatically charged overnight (-1.2 V versus Hg/HgO). Typical charge and discharge curves for electrode TFE-4
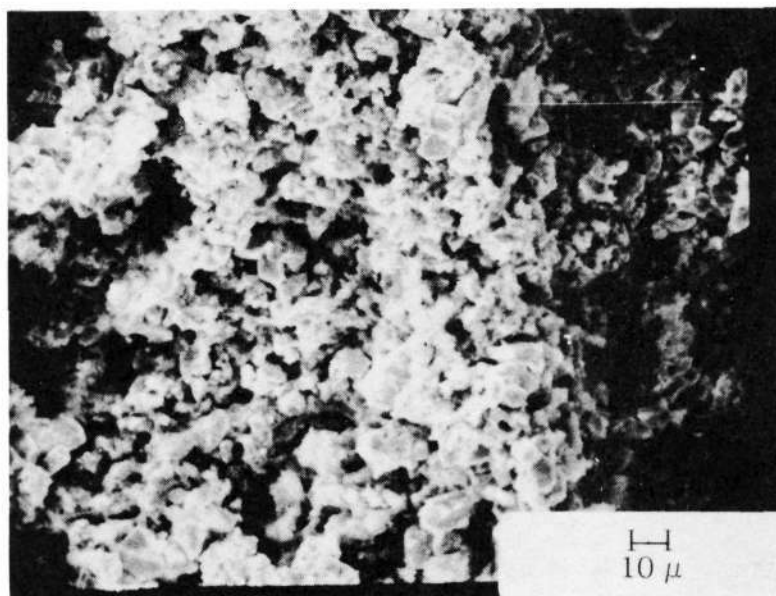
Fig. 29. Cycled Cd-impregnated Ni sinter (NS Cd-4, 73 cycles, 60% discharged)

are shown in Fig. **30.** The capacity as a function of cycle number is shown in Table VII. The capacities compared very well with those of electrode TFE-**3** which had the same composition.

Table VII. Capacity of Teflon Bonded Cd Electrode TFE-**4,** (Room Temperature, 25% KOH Cycled Between -775 mV and -1275 mV vs Hg/HgO)

No. of Cycles	Discharge Time, hr	Capacity, % of Theoretical
2	2.70	64.0
5	1.85	49.0
10	1.08	29.0
20	1.45	22.5
40	3.13	17.0
Potentiostated to -1.2 V vs Hg/HgO for 18 hr		
50	2.42	26.0
75	1.35	14.0

Typcial charge-discharge cycles of TFE Cd-**1** are shown in Fig. **31.** The advent of gas evolution occurred at -1.28 V versus Hg/HgO which was approximately 70 mV cathodic than with silver containing Teflon-bonded electrodes. The measured capacities (as a fraction of the theoretical capacity) are listed in Table VIII. The utilization of active material in this electrode was particularly low. This may have been due to the fairly loose structure particular to this electrode (it was not pressed) or to a contact problem with the expanded cadmium substrate. Further experiments on Teflon-bonded electrodes using cadmium substrates will be necessary to clarify this question.

A scanning electron micrograph of this electrode after cycling showed distinct hexagonal crystals (Fig. **32**).

Fig. 30. Charge and discharge cycles of Teflon-bonded Cd electrode TFE-4 (cycle no. 48, 4 mA/cm² 25% KOH, room temperature, a = first individual small bubbles; b = weak gassing; c = steady gassing)
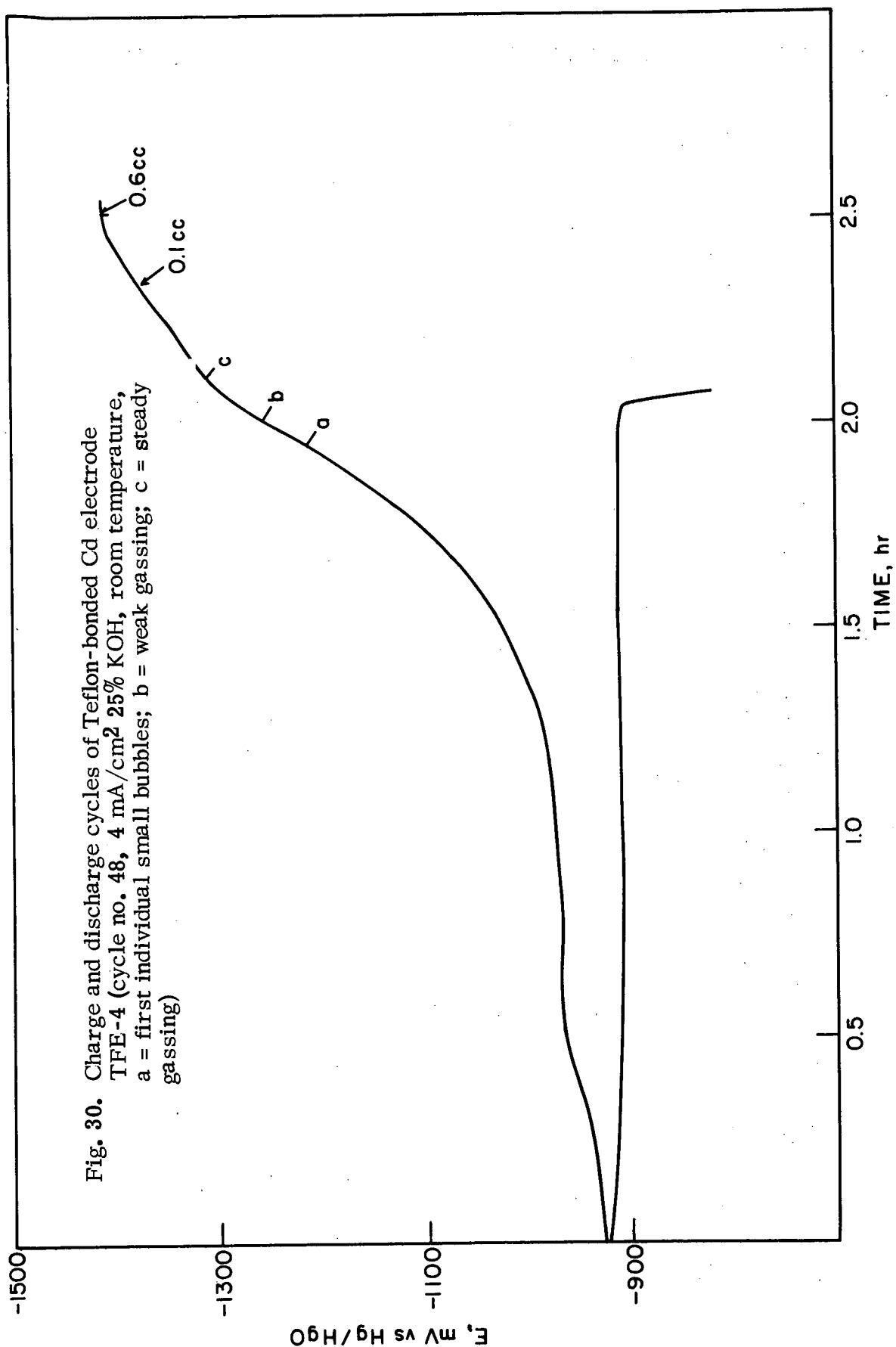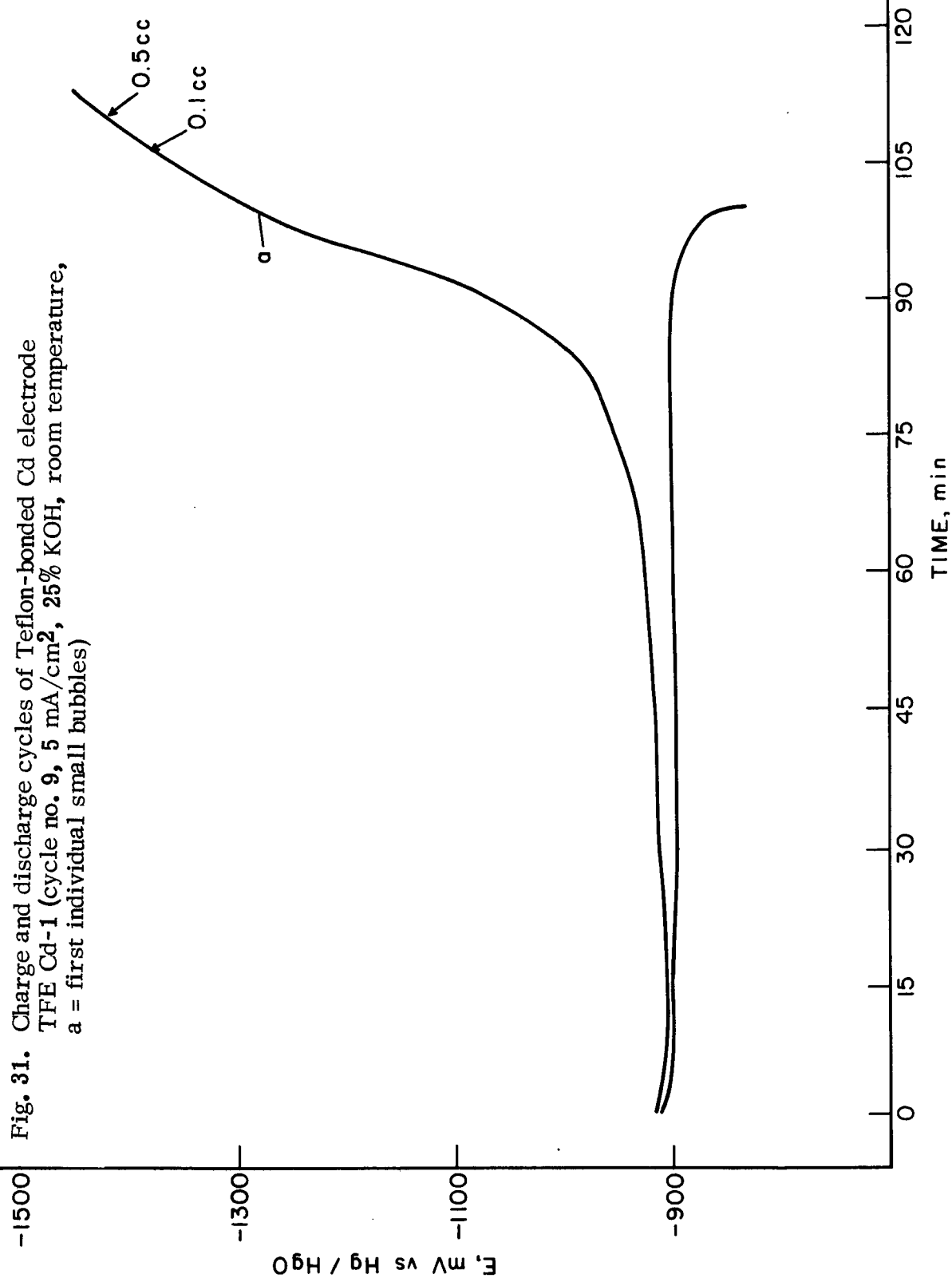
Fig. 31. Charge and discharge cycles of Teflon-bonded Cd electrode
TFE Cd-1 (cycle no. 9, 5 mA/cm², 25% KOH, room temperature,
a = first individual small bubbles)

10 μ
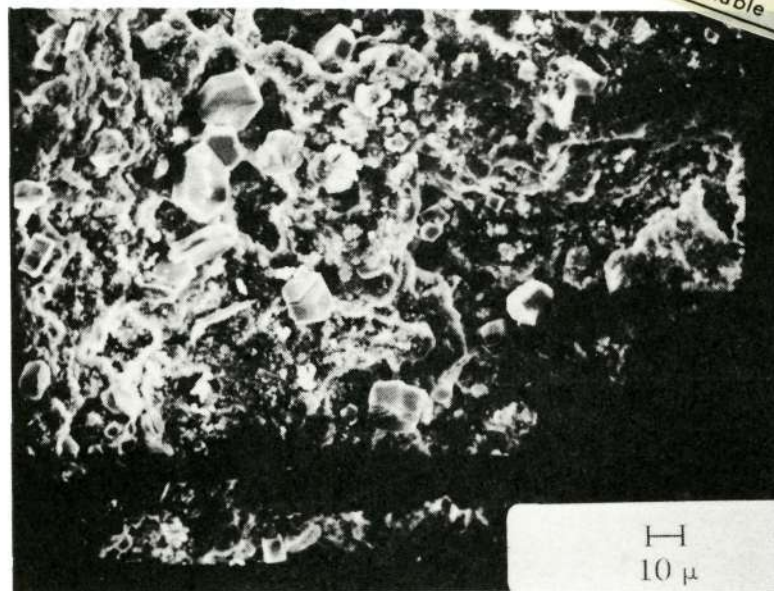
Fig. 32. Cycled Teflon-bonded electrode TFE Cd-1 (85 cycles, discharged)

Table VIII. Capacity of Teflon Bonded Cd Electrode TFE Cd-1, (Room Temperature, 25% KOH Cycled Between -775 mV and -1275 mV vs Hg/HgO)

No. of Cycles	Discharge Time, hr	Capacity, % of Theoretical	
1	2.16	18.5	
3	1.40	8.0	
5	3.40	26.0	(charge to H_2
10	1.28	10.0	evolution)
30	0.62	4.7	
50	0.56	4.3	
60	0.56	4.3	
Potentiostated to -1.2 V vs Hg/HgO for 24 hr			
65	0.76	5.9	
85	0.59	4.3	

C. Electrodeposited Sponge Cadmium

1. Cd sponge preparation

Our experiments were based on the results of an investigation by Henderson and Ladan[2] on the preparation and structure of electrodeposited cadmium sponge. Depending on experimental conditions, deposits of different morphology were reported. For a high electrochemical efficiency, the deposit must be present in a very fine state of subdivision. In addition, the deposit must be sufficiently porous to facilitate bulk transport to and from the electrode during cycling and at the same time should be very adherent to the substrate.

The plating bath consisted of 100 g $CdCl_2$ and 130 KCl in 1 ℓ of triply distilled water. The electrodeposition of cadmium was carried out at room temperature in a glass container. Two cadmium counterelectrodes were located parallel and equidistant to the substrate, for which expanded cadmium metal and cadmium sheet (5 and 10 mil) were used with various surface pretreatments. Table IX summarizes the results. The morphology of the deposits varied between spongy and crystalline. The surface treatment of the substrate and thus the creation of suitable nucleation sites appeared to be of central importance. An example of a crystalline Cd deposit is shown in Fig. 33. Such deposits have a relatively low surface area and correspondingly low efficiencies when subjected to charge and discharge cycles. Fig. 34 shows a high surface area sponge with a dark grey appearance (sample No. 9).

Table IX. Electrodeposition of Sponge Cadmium on Cadmium (Solution: 100 g $CdCl_2$ + 130g CdCl/ℓ, Room Temperature)

Sample No.	Surface Preparation	i, mA/cm^2	Time, min	Deposit Morphology
1 (Cd Screen)	Reduced in 30% KOH H_2O rinse	10	6	Crystalline
2		35	15	
3		5	45	
4 Cd sheet		30	20	Fine crystalline
5		30	35	Small area of sponge rest crystalline
6		30	50	Variable both types
7	Detergent wash H_2O rinse	30	20	Crystalline
8	Hand polished with alumina H_2O rinse	10	60	Good sponge poor adherence
9		60	60	Good sponge poor adherence
10		10	60	Crystalline
11		10	-	Variable results
12	Rinsed in KOH-ethyle alcohol misture (50-50 w/25% KOH)	20	120	
13	Anodic-cathodic treatment in 25% KOH	20	120	
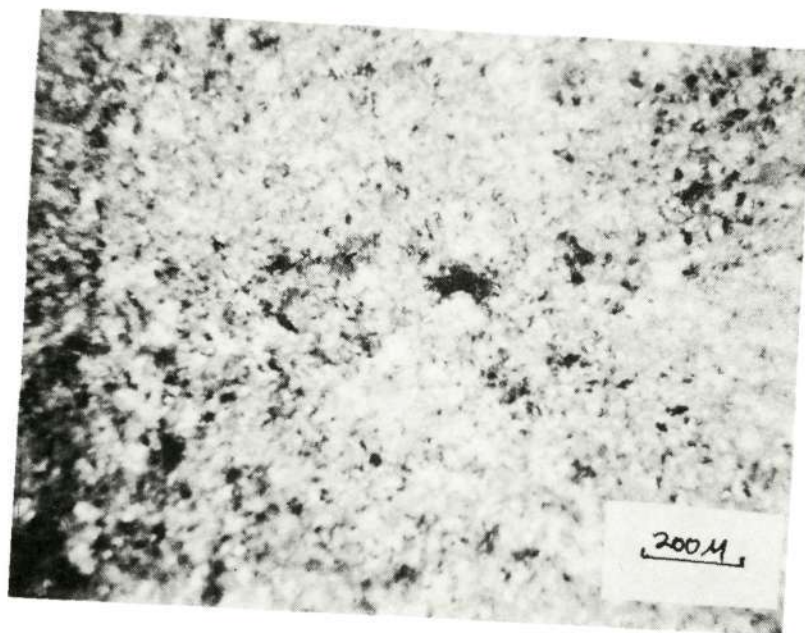
Fig. 33. Electrodeposited crystalline cadmium
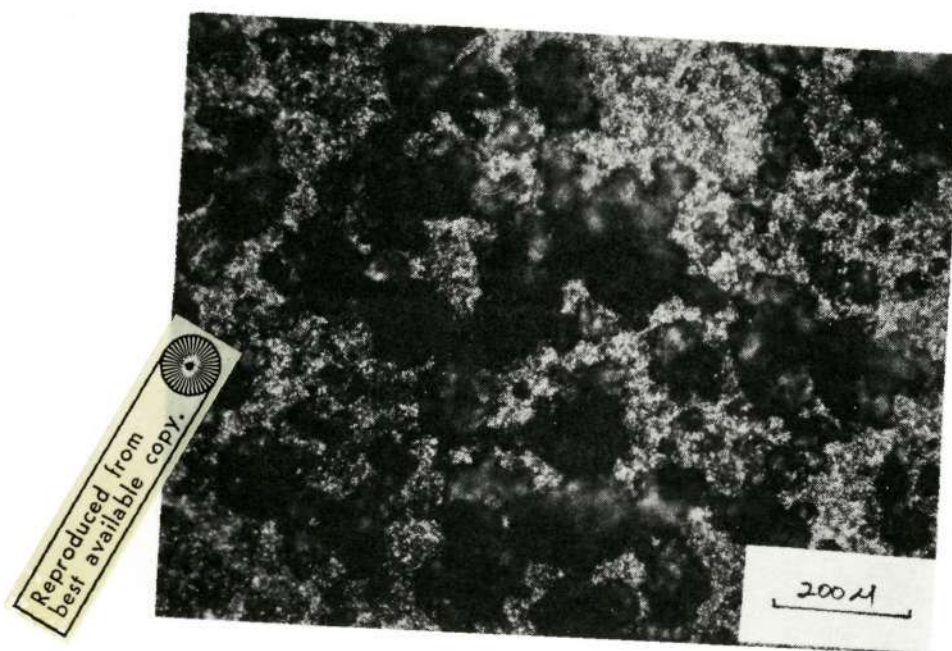
Fig. 34. Electrodeposited Cd sponge

2. Electrochemical evaluation

A cadmium deposit of similar appearance to the one shown in Fig. 34, was subjected to electrochemical testing. The electrode was cycled at room temperature between -1.24 V and -0.75 V versus a Hg/HgO reference electrode. Fig. 35 shows a typical charge-discharge cycle. At the end of charge, we observed a large potential change to hydrogen evolution. The advent of gas evolution occurred at approximately -1.3 V versus Hg/HgO.

The utilization and the change in capacity as a function of the number of charge and discharge cycles is shown in Table X. As in our previous tests, we found a decrease in capacity with cycling. Extending the charge cycle to hydrogen evolution or holding the electrode potentiostatically at -1.2 V versus Hg/HgO increased the capacity considerably. The mechanical stability of the plated sponge was only moderately good, showing significant shedding during cycling.

Table X. Capacity of Electrodeposited Cd-Sponge Electrode ES Cd-1, (Room Temperature, 25% KOH Cycled Between -840 mV to -1270 mV vs Hg/HgO Reference)

No. of Cycles	Discharge Time, hr	Capacity, % of Theoretical
1	3.04	54.5
2	2.90	52.0
5	1.04	37.0
10	0.86	31.0
45	0.98	17.0
		Full charge
50	1.79	32.0
60	1.19	21.0
100	1.02	18.5
175	0.95	16.0
Potentiostated to -1.2 vs Hg/HgO for 60 hr		
178	2.85	51.0
180	2.00	36.0
183	1.68	30.2
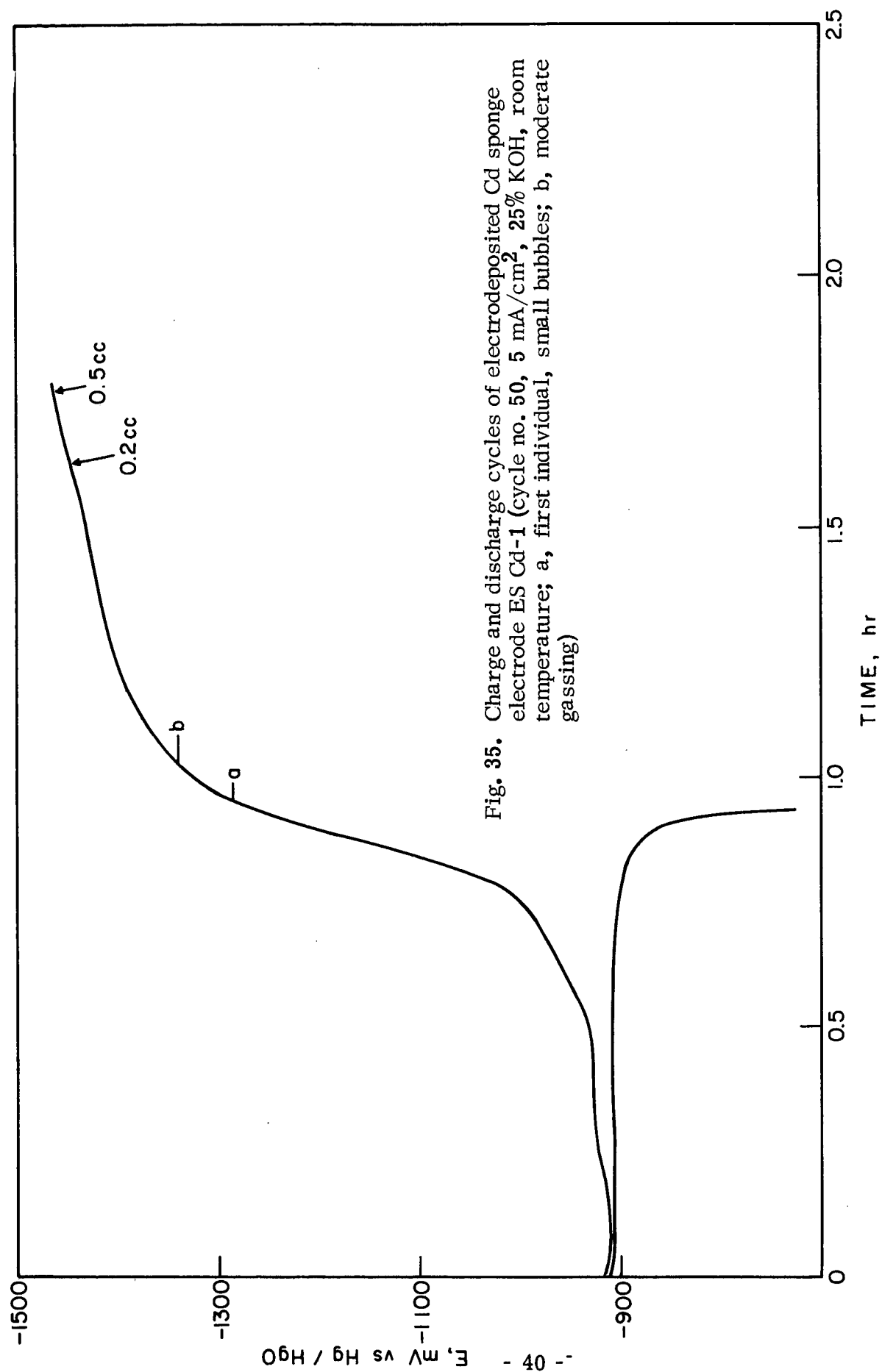
Fig. 35. Charge and discharge cycles of electrodeposited Cd sponge electrode ES Cd-1 (cycle no. 50, 5 mA/cm^2, 25% KOH, room temperature; a, first individual, small bubbles; b, moderate gassing)

- 40 -

D. Cadmium Sinter Based Structures

1. Preparation of Cd sinters

A feasibility study of manufacturing procedures for Cd-sinter-based structures was carried out using high purity Cd (59 Cominco American) of different particle size. This material came from the same production lot (HPM 1185) and was classified according to ASTM screen fractions. We characterized the material further as shown in Table XI.

Table XI. Cadmium Powder Characteristics

Screen Size	Fischer Average Particle Diameter, μ	Bulk Density, g/cc	Packed Density, g/cc
-100	41	2.35	2.99
-200	30	2.66	3.51
-325	14	2.48	3.46

Scanning electron microscope pictures of Cd-200 and Cd-325 powders are shown in Figs. 36 and 37. The powders were irregularly shaped, especially in the case of Cd-325 and covered a wide range of particle sizes.

In an effort to obtain cadmium plaques, we investigated the sintering of cadmium powders (a) in argon, (b) in hydrogen-helium mixtures, (c) in the presence of a flux, and (d) in the form of Cd-NaF compacts.

    a. Sintering experiments in Ar: Initial sintering experiments were carried out on loose layups in a high purity Ar atmosphere. Since cadmium oxide has an appreciable vapor pressure, it was hoped that the oxide coating on the surface of the powders might evaporate enabling the cadmium metal to sinter together. However, no significant sintering was observed at temperatures up to 300° C.

    b. Sintering under hydrogen: Experiments were carried out in a reducing atmosphere using a 15% H_2-85% He gas mixture. Here again practically no sintering was observed with the powder showing a reddish brown discoloration. It appeared that the powders contained a considerable amount of oxide and in addition possibly occluded oxygen. This was probably a consequence of the production of these powders by a fluidized energy technique with air as propellent.
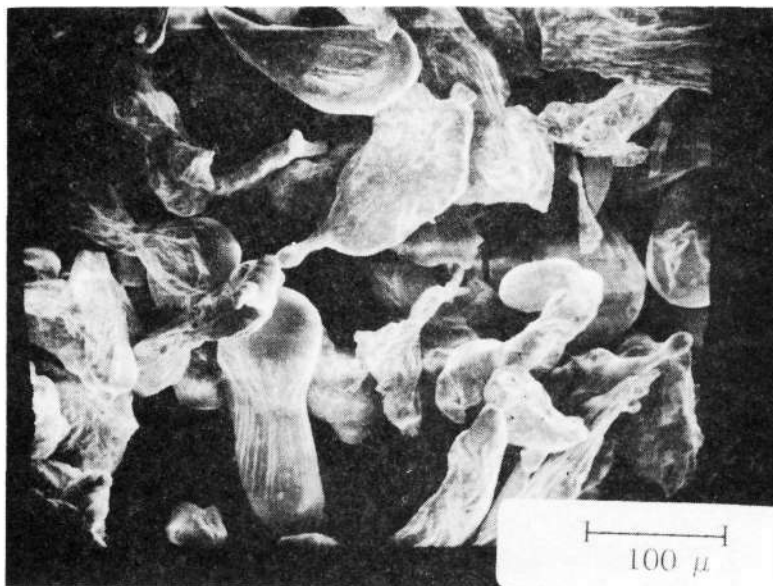
Fig. 36. Cadmium powder Cominco-200
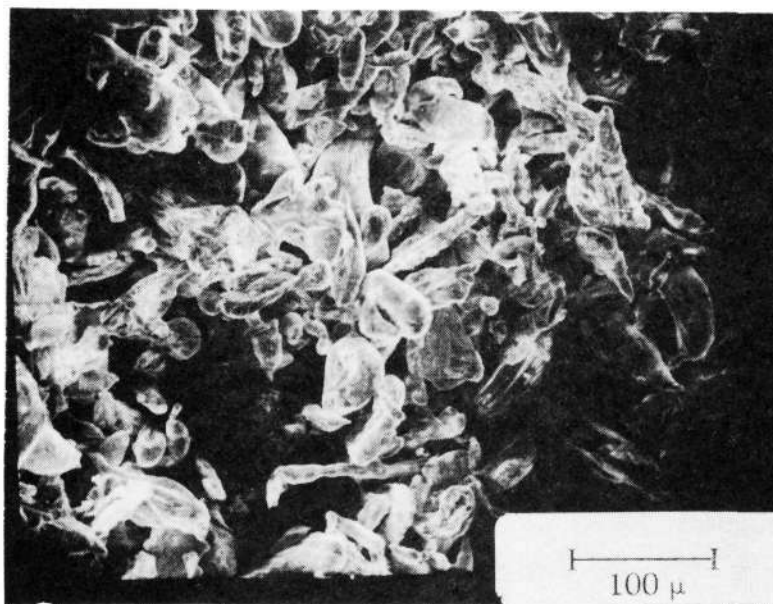
Fig. 37. Cadmium powder Cominco-325

c. <u>Sintering in the presence of flux:</u> This approach consisted of the use of a flux in order to create suitable surfaces for cadmium interdiffusion. We experimented with a liquid flux (No. 30, Superior Flux Co.). By wetting a dry layup of -325 cadmium powder with the flux and heating it in the hydrogen-helium mixture for 30 min to 300°C, we were able to sinter the cadmium particles together. A close examination showed however that a plastic-like flux residue was not completely removable by treatment with solvents such as, water, alcohol, carbon tetrachloride or hexane.

d. <u>Sintering of Cd-NaF compacts:</u> Samples of 1 1/4-in. diameter were obtained by compacting a mixture of 60 vol% NaF and 40 vol% of -325 Cd powder at 20400 lb/in.^{2}. Compacts heated for 30 min to 300°C in an argon atmosphere disintegrated upon leaching. It was hoped that the compacting would create a sufficiently close contact between the cadmium particles and possibly expose also some fresh surfaces, thus enhancing interdiffusion and sintering. Porous cadmium structures were, however, successfully produced by the following procedures:

1. A Cd-NaF compact as described above was heated slightly beyond the melting point of Cd. After leaching, a mechanically sound structure of porous cadmium remained. A fractured cross section is shown in the scanning electron micrograph of Fig. 38. It is worth noting the extremely rugged internal surface of this structure.

2. This procedure is characterized by the addition of an inorganic salt which will melt below the desired sintering temperature and can act as a flux by dissolving the cadmium oxide. To explore this approach, the eutectic melt of 50 mol% KNO_3 and 50 mol% $NaNO_3$ (MP 220°C) was ground to a fine powder and 5% by weight was added to the NaF-Cd mixture. After thorough blending, the mixture was compacted (18,500 psi for 5 min). The resulting structure, after leaching, exhibited reasonable mechanical strength. A scanning electron micrograph of a cross section is shown in Fig. 39. The actual structure of the cadmium sinter was masked by cadmium hydroxide crystals which precipitated upon leaching.

2. Electrochemical evaluation of Cd-sinter structures

A cadmium sinter plaque obtained by leaching of a NaF-compact (preparation method 2) was impregnated with cadmium hydroxide equivalent to a theoretical capacity of 0.125 Ahr and cycled at room temperature in 25% KOH. The capacity of this electrode (CdS-1) as a function of cycle number is shown in Table XII. The measured capacity continuously increased as a larger part of the cadmium sinter
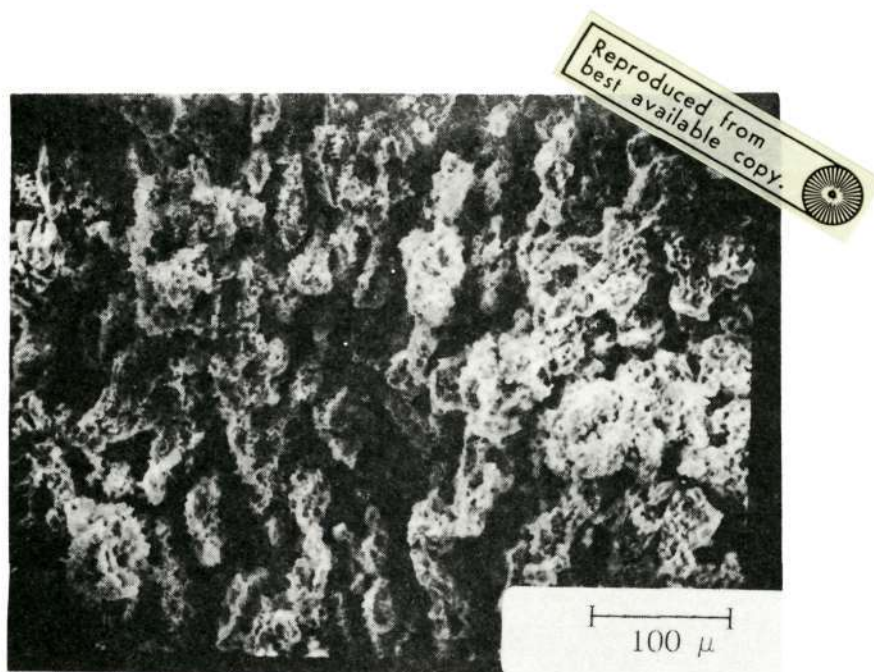
Fig. 38. Cadmium sinter (preparation method 1)
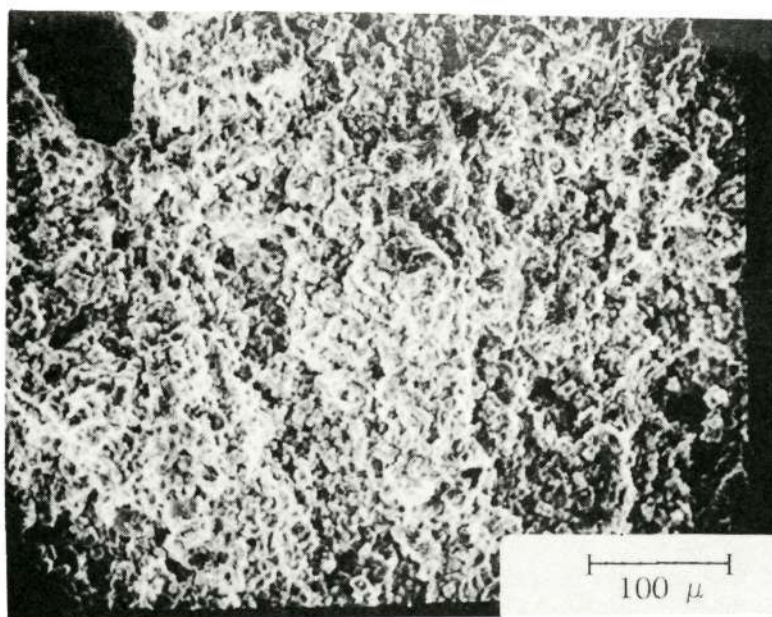
Fig. 39. Cadmium sinter (preparation method 2)

Table XII. Capacity of Cd Sinter Based Cd Electrode Cd S-1 (Room Temperature, 25% KOH, 7.4 cm^2, 40 mil)

No. of Cycles	Discharge, hr	Capacity, Ahr	Comments
1	1.70	0.340	25.6 mA/cm^2; cycled from -850 mV to -1250 mV vs Hg/HgO
5	1.68	0.336	
10	1.50	0.300	
20	1.58	0.316	
30	1.84	0.368	
40	1.94	0.388	
50	1.08	0.216*	
60	2.15	0.430	
100	2.62	0.524	
120	2.74	0.548 Utilization 49% of plate weight	
130	2.80	0.560	
140	1.71	0.513	38.5 mA/cm^2; cycled as above
160	1.71	0.513 Electrode swollen, shedding	
180	1.47	0.442	
195	1.34	0.402 Electrode disintegrating	

* at 5°C.

structure participated in cycling. After approximately 130 cycles, a maximum capacity was reached corresponding to over 50% utilization based on the total plate weight. After that, the capacity remained fairly constant until the electrode slowly disintegrated. This type of electrode disintegration should not be a significant problem in the constrained configuration of an actual battery. Typical charge and discharge cycles of this electrode are shown in Fig. 40. The charge and discharge plateaus are fairly flat, the charge plateau being followed by a large potential change prior to the end of charge. The advent of gas evolution occurred at -1.3 V versus Hg/HgO. After cycle 49, the cell was cooled to 5°C. A typical cycle at that temperature is also shown in Fig. 40. There is little difference in shape between the cycles at 23°C and 5°C. However, at the same current density, the capacity at 5°C is only approximately 2/3 of the value at 23°C. The advent of hydrogen evolution at 5°C occurs at approximately -1.4 V versus Hg/HgO.

Fig. 41 represents a scanning electron micrograph of the electrode CdS-1 after cycling. It shows the wide size distribution of the $Cd(OH)_2$ crystals.

Fig. 40. Charge and discharge cycles of Cd sinter electrode Cd S-1 (25.3 ma/cm$_2$, 30 % KOH; A, cycle 49 at 25° C; a, advent of gas evolution; b, moderate gassing; c, strong gassing)

10 μ
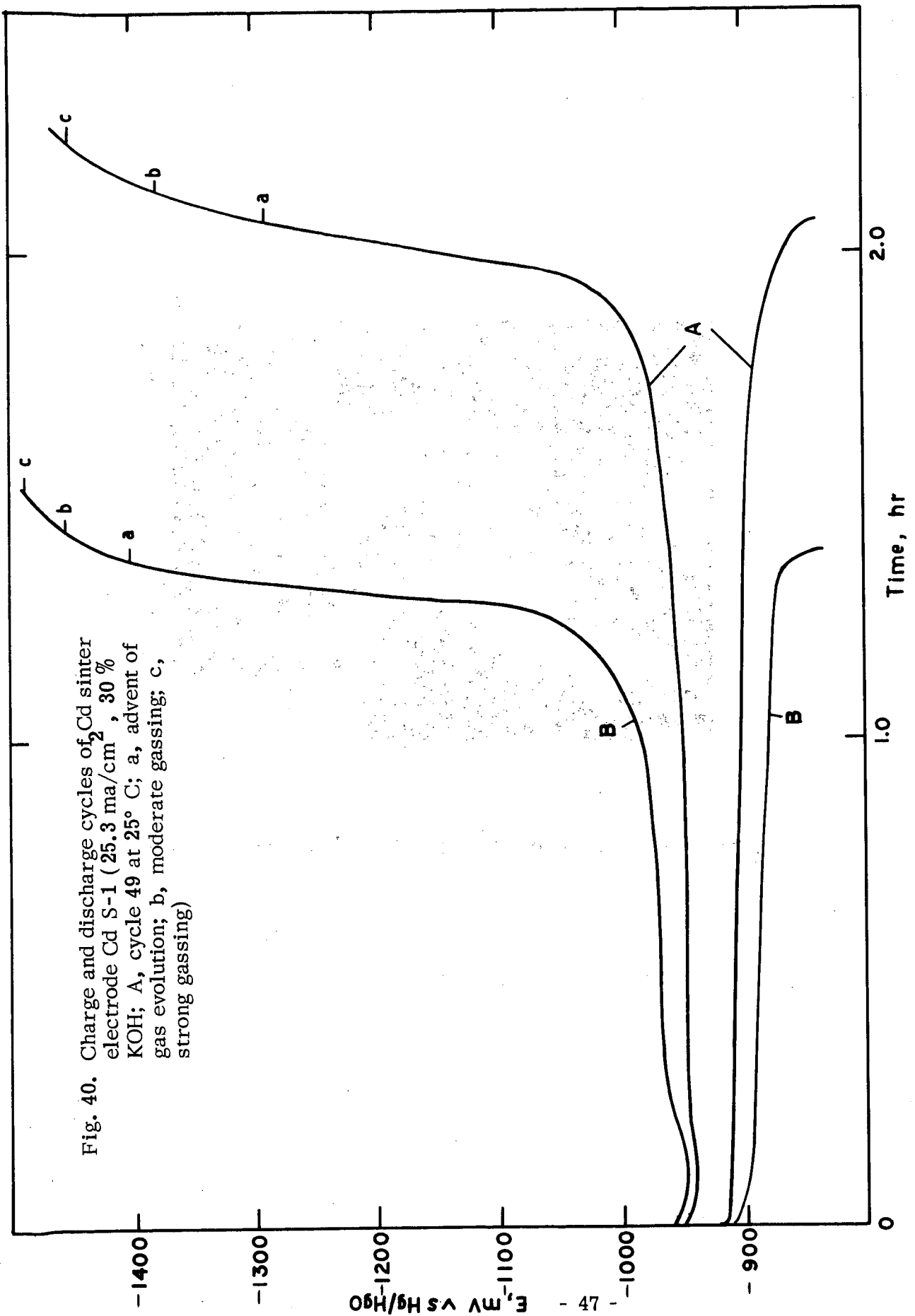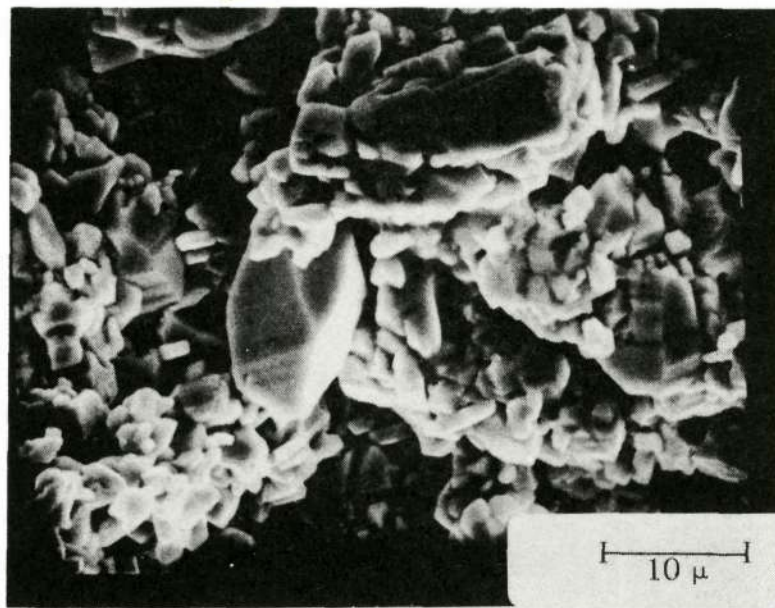
Fig. 41. Cycled Cd-sinter electrode Cd S-1 (196 cycles, discharged)

III. FUTURE WORK

We will continue in the development of the various plaque structures proposed for negative plates and concentrate specifically on investigating further fabrication techniques and electrochemical behavior of Teflon-bonded Cd electrodes. To obtain the data necessary for successful cell constructions, such as the effect of temperature and charge rate, we will carry out a test program for various positive and negative plates at three different temperatures and at three charge rate levels. The measured parameters for positive plates will be: (1) electrode potential, (2) capacity, and (3) O_2 evolution rate as a function of state of charge. For negative plates, we will measure: (1) electrode potential, (2) capacity, and (3) the advent of hydrogen evolution.

IV. REFERENCES

1. NiCd Battery Electrodes, First Quarterly Report by Tyco Laboratories, Inc. for Jet Propulsion Laboratory under Contract No. 953185-NAS7-100.

2. I.H.S. Henderson and S.G. Ladan, Canadian Journal of Chemical Engineering, **46**, 355, (1968).

C.2

APPENDIX

Additional Experimental Data on
Silver-Sinter-Based Cd Electrodes

Table A-I. Capacity of Silver-Sinter-Based Cd Electrode SS Cd-2
(130 Compact, Room Temperature, 25% KOH)

No. of Cycles	Discharge, hr	Capacity, % of Theoretical	Comments
1	0.88	42.0	18.6 mA/cm^2; cycled -775 to -1250 versus Hg/HgO no gas evolution
3	0.56	27.0	
5	0.42	21.0	
10	0.28	13.0	
20	0.18	9.0	
30	0.29	7.0	9.3 mA/cm^2; cycled same as above; no gas evolution
37	0.20	5.0	

Potentiostated to -1.2 versus Hg/HgO for 63 hr

No. of Cycles	Discharge, hr	Capacity, % of Theoretical	Comments
38	0.91	22.0	
40	0.52	13.0	
45	0.28	6.6	
50	0.18	4.2	
75	0.08	1.8	
100	0.06	1.3	
155	0.04	1.1	

Table A-II. Capacity of Silver-Sinter-Based Cd Electrode SS Cd-3
(Ag 220, Dry Layup, Room Temperature, 25% KOH)

No. of Cycles	Discharge, hr	Capacity, % of Theoretical	Comments
1	1.85	54.0	14 mA/cm^2; cycled
3	0.90	34.0	-775 to -1250 versus Hg/HgO; no gas
5	0.62	29.0	evolution
10	0.45	21.0	
19	0.34	15.5	
20*	0.48	22.0	
30	0.54	12.0	7 mA/cm^2; cycled
40	0.35	8.0	same as above; no gas evolution
48	0.34	7.7	

*Charged to -1.47 V

Table A-III. Capacity of Silver-Sinter-Based Cd Electrode SS Cd-4
(Ag 130, Dry Layup, Room Temperature, 25% KOH)

No. of Cycles	Discharge, hr	Capacity, % of Theoretical	Comments
1	0.68	42.5	12 mA/cm^2; cycled -725 to -1275 mV versus Hg/HgO; no gas evolution
5	0.44	27.5	
10	0.32	20.0	
15	0.25	15.6	
20	0.20	12.5	
25	0.16	10.0	
30	0.13	8.1	
45	0.10	6.2	
47	0.37	23.1	Cycled -725 to -1475 mV versus Hg/HgO; some gas evolution
50	0.32	20.0	
60	0.24	15.0	
75	0.19	11.9	
100	0.16	10.0	

Table A-IV. Capacity of Silver-Sinter-Based Cd Electrode SS Cd-5
(Ag 150, FAPD 15.2μ; Dry Layup, Room Temperature,
25% KOH)

No. of Cycles	Discharge, hr	Capacity, % of Theoretical	Comments
1	1.10	49.3	11.5 mA/cm^2; cycled
5	0.74	33.2	-750 to -1300 mV versus Hg/HgO;
10	0.50	22.4	negligible gas evolution
15	0.38	17.0	
25	0.25	11.2	
35	0.18	8.1	
50	0.14	6.3	
59	0.41	18.4	Cycled -750 to -1475
60	0.40	17.9	mV; some gas evolution
65	0.38	17.0	
68	0.38	17.0	

Table A-V. Capacity of Silver-Sinter-Based Cd Electrode SS Cd-6
(Ag 220, Dry Layup, Room Temperature, 30% KOH)

No. of Cycles	Discharge, hr	Capacity, % of Theoretical	Comments
1	0.38	28.5	10 mA/cm^2; 100% overcharge
2	0.35	26.4	
3	0.32	24.0	
4	0.28	21.0	
5	0.25	18.8	
6	0.70	26.3	5 mA/cm^2; 100% overcharge
10	0.52	19.5	5 mA/cm^2; cycled -775 to -1325 mV versus Hg/HgO
20	0.26	9.8	
30	0.19	7.1	
40	0.16	6.0	
45	0.32	6.0	2.5 mA/cm^2; cycled same as above
55	0.29	5.5	
80	0.17	3.2	

Table A-VI. Capacity of Silver-Sinter-Based Cd Electrode SS Cd-7
(Ag 220, Dry Layup, Room Temperature 30% KOH)

No. of Cycles	Discharge, hr	Capacity, % of Theoretical	Comments
1	0.52	38.8	10 mA/cm^2, 100% overcharge
2	0.47	35.0	
3	0.44	32.8	
4	0.40	29.8	
5	0.36	26.8	
6	0.98	36.5	5 mA/cm^2; cycled -775 mV to
10	0.59	22.0	-1325 mV vs Hg/HgO
25	0.24	9.0	
35	0.42	7.8	2.5 mA/cm^2; cycled same as
45	0.32	6.0	above
55	0.24	4.5	
80	0.18	3.4	

Table A-VII. Capacity of Silver-Sinter-Based Cd Electrode SS Cd-8
(Ag 220, Dry Layup, Modified, Room Temperature,
30% KOH)

No. of Cycles	Discharge, hr	Capacity, % of Theoretical	Comments
1	2.13	74.6	5 mA/cm^2, cycled -725 mV to -1375 mV vs Hg/HgO
5	1.52	53.5	
10	1.08	38.0	
20	0.66	23.2	
30	0.52	18.3	
40	0.43	15.5	
50	0.38	13.4	
75	0.29	10.0	
91	1.45	20.4	2 mA/cm^2; previous cycle to gas evolution
95	0.82	11.5	
100	0.68	9.6	
115	0.58	8.2	

Table A-VIII. Capacity of Silver-Sinter-Based Cd Electrode SS Cd-9
(Ag 220, Dry Layup, Modified, Room Temperature
30% KOH)

No. of Cycles	Discharge, hr	Capacity, % of Theoretical	Comments
1	1.88	67.6	5 mA/cm^2; cycled -725 mV to -1375 mV vs Hg/HgO
5	1.40	50.4	
10	1.12	40.3	
20	0.74	26.6	
30	0.58	20.9	
50	0.39	14.0	
60	0.89	14.0	2 mA/cm^2; cycled same as above
75	0.44	6.3	
100	0.28	4.0	

Table A-IX. Capacity of Silver-Sinter-Based Cd Electrode SS Cd-10
(Ag 220, Dry Layup, Modified, Room Temperature
30% KOH)

No. of Cycles	Discharge, hr	Capacity, % of Theoretical	Comments
1	1.58	74.5	7.8 mA/cm^2; cycled -725 mV to -1325 mV vs Hg/HgO
5	1.14	53.7	
10	0.86	40.5	
20	0.54	25.4	
30	0.43	20.3	
40	0.35	16.5	
50	0.30	14.1	
60	0.75	16.5	3.9 mA/cm^2; cycled same as above
68	0.52	12.2	
80	0.43	10.0	
100	0.30	7.1	
118	0.60	5.7	1.5 mA/cm^2

Table A-X. Capacity of Silver-Sinter-Based Cd Electrode SS Cd-11
(Ag **300**, Dry Layup, Room Temperature, 30% KOH)

No. of Cycles	Discharge, hr	Capacity, % of Theoretical	Comments
1	2.33	72.0	5 mA/cm^2; cycled -725 mV to
5	1.44	44.5	-1325 mV vs Hg/HgO
10	1.00	30.8	
20	0.60	18.5	
30	0.44	13.6	
40	0.37	11.4	
50	0.32	9.9	
60	0.29	9.0	
80	0.70	10.0	2.5 mA/cm^2
100	1.53	9.4	1.0 mA/cm^2
110	1.02	6.3	

Table A-XI. Capacity of Silver-Sinter-Based Cd Electrode SS Cd-12
(Ag 300, Dry Layup, Room Temperature, 30% KOH)

No. of Cycles	Discharge, hr	Capacity, % of Theoretical	Comments
1	1.85	74.5	5 mA/cm^2; cycled -725 mV to -1325 mV vs Hg/HgO
5	1.21	48.8	
10	0.85	34.2	
20	0.56	22.6	
30	0.41	16.5	
40	0.35	14.1	
50	0.30	12.1	
60	0.27	10.9	
70	0.25	10.1	
90	0.48	19.3*	2.5 mA/cm^2; cycled same as above
110	0.43	8.7	
130	0.38	8.4	
145	0.82	7.3	1.0 mA/cm^2

* Cycle No. 80 charged to H_2 evolution

Table A-XII. Capacity of Silver-Sinter-Based Cd Electrode SS Cd-13
(Ag 300, Dry Layup, Room Temperature, 30% KOH)

No. of Cycles	Discharge, hr	Capacity, % of Theoretical	Comments
1	2.05	70.0	5 mA/cm^2; cycled -725 mV to -1325 mV vs Hg/HgO
5	1.33	45.5	
10	0.92	31.5	
20	0.54	18.5	
30	0.41	14.0	
40	0.34	11.6	
50	0.32	11.0	
60	0.26	8.9	
70	0.88	15.0	2.5 mA/cm^2; cycled same as above
80	0.64	11.0	
100	1.00	6.9	1.0 mA/cm^2